The Noise from Isotropic Turbulence

Steven A. E. Miller*

Turbulence naturally returns to isotropy and often possesses locally isotropic regions. This paper presents a new method to predict noise from turbulence that has returned or is returning to isotropy. The Navier-Stokes equations are decomposed into anisotropic and isotropic turbulent components and corresponding radiating waves. An analytical solution is proposed for the radiating waves associated with isotropic turbulence that contains arguments involving the vector Green's function of the Navier-Stokes equations and the multi-order two-point cross-correlation of the Navier-Stokes equations involving turbulent fluctuations. Using the theory of isotropic turbulence, the two-point cross-correlation of the Navier-Stokes equations is written as a vector-normalized, two-point cross-correlation multiplied by corresponding wavenumber spectra of the structure functions. Composite structure functions of the field variables are adapted from canonical theory of isotropic turbulence. The vector-normalized two-point cross-correlation involves arguments of separation distance, wavenumber, and corresponding turbulent length and time scales. A solution of the vector Green's function of the linearized Navier-Stokes equation for acoustic pressure is derived. A simple system of differential and algebraic equations is proposed to model the statistics of stationary and decaying isotropic turbulence, which are arguments of the model equation. Predictions of acoustic and turbulent statistics are compared with a wide variety of measurements and direct numerical simulations from various sources over a range of Reynolds numbers and initial scales. Predictions compare favorably with previous theories, direct numerical simulations, and measurements.

Nomenclature

Symbols	Description
c	Speed of sound
c_i	Constants
c_p	Specific heat at constant pressure
c_v	Specific heat at constant volume
E_i	Spectra of 'i'
e	Energy
f	Frequency
k	Turbulent kinetic energy
L	Integral length scale
$\mathcal{L}$	Characteristic length scale
l	Turbulent length scale
P_a	Acoustic power
p	Pressure
q	Arbitrary field variables
q_g	Vector Green's function
$\boldsymbol{R}$	Normalized two-point cross-correlation
$R_{m,n}$	Two-point cross-correlation of $\boldsymbol{\Theta}$
R	Gas constant
$\boldsymbol{r}$	Vector from source to observer
S_k	k^{th} Spectral density
T	Temperature
$\mathcal{T}$	Integral time scale
t	Time
$\boldsymbol{u}$	Velocity vector
u	Turbulent velocity scale
$\boldsymbol{x}$	Observer vector
$\boldsymbol{y}$	Source vector
$\boldsymbol{z}$	Source vector

Greek Symbols	
γ	Ratio of specific heats
δ	Dirac delta function
δ_{ij}	Kronecker delta function
ϵ	Dissipation
η	Kolmogorov scale
$\boldsymbol{\eta}$	Separation vector
$\boldsymbol{\Theta}$	Source vector
ι_c	Constant coefficient
κ	Wavenumber
μ	Dynamic viscosity
ν	Kinematic viscosity
ρ	Density
τ	Retarded time or turbulent time scale
ω	Radial frequency

Non-Dimensional Numbers	
$\mathcal{M}_t$	Turbulent Mach number
$\mathcal{P}r$	Prandtl number
$\mathcal{R}e_L$	Integral Reynolds number
$\mathcal{R}e_t$	Turbulent Reynolds number
$\mathcal{R}e_\lambda$	Taylor Reynolds number
$\mathcal{S}t$	Strouhal number

Abbreviations	
CFD	Computational fluid dynamics
DNS	Direct numerical simulation
LES	Large eddy simulation
PSD	Power spectral density
SPL	Sound pressure level

*Assistant Professor, The Department of Mechanical and Aerospace Engineering, The University of Florida, 231 MAE-A, P.O. Box 116250, Gainesville, FL, 32611, USA, AIAA Senior Member, saem@ufl.edu; saemiller@gmail.com

Introduction

The physical understanding of turbulence and the mechanism of how sound is radiated by turbulence remain open problems. Turbulence and associated acoustic radiation are found throughout nature and in the presence of almost all aerospace vehicles. Turbulent flows often return to isotropy or in the very least can be characterized to have local spatially isotropic regions. Here, regions of a turbulent field are classified as either locally anisotropic or isotropic. The wavenumber 'energy' spectra of the field variables in a turbulent fluid that is returning or has returned to isotropy possess a universal behavior. This paper presents a new method to predict noise from turbulence that has returned to isotropy based upon the wavenumber spectra of the Navier-Stokes equations.

Taylor,[1] in perhaps his greatest paper on the theory of turbulence, writes, '*in isotropic turbulence the average value of any function of the velocity components, defined in relation to a given set of axes, is unaltered if the axes of reference are rotated in any matter.*' Turbulent flows have a strong tendency to become isotropic, and indeed this philosophy is attributed to Kolmogorov,[2–4] who made popular the term, '*return to isotropy.*' Isotropic turbulence is observed within grid turbulence (where it is mostly studied experimentally), away from the wall of a turbulent boundary layer, in the atmosphere far from the ground, within bounded fully developed flows such as pipes, within the plume of a high speed jet, and in many other flows. The concept of isotropy is not limited to fluids (e.g., gases, liquids, and plasmas) but is also apparent in the cosmic background radiation (see Readhead and Lawrence[5] for example). Excellent visualizations of isotropic turbulence are rare because of the difficulty of measurement. In Fig. 1 a) a schlieren and b) a shadowgraph of isotropic turbulence are shown by Hesselink and Sturtevant[6] where a shock wave is moving from left to right. Here, the 'random' medium is the isotropic turbulence, and the very thin vertical disturbance is the shock wave. The self-similarity and self-preservation concepts of turbulent flow are central theories within this work. There is a tremendous amount of research available on turbulence, and readers can familiarize themselves with these concepts through the works of Stewart and Townsend,[7] Sreenivasan and Antonia,[8] Ishihara et al.,[9] and Pope.[10]

Wavenumber energy spectra of structure functions play a key role in contemporary turbulence theory and in the development of the mathematical model of this paper. Perhaps the only exact result in statistical fluid mechanics is due to the brilliance of Kolmogorov[2–4] (K41 theory). Of specific importance, Kolmogorov shows that the three-dimensional energy spectrum of the velocity structure function is proportional to $c_u \epsilon^{3/2} \kappa^{-5/3}$ in the inertial range, where c_u is a constant, ϵ is the dissipation, and κ is the wavenumber. Remarkably, two decades later the theory was slightly altered by Kolmogorov[11] (K62 theory) to account for intermittency. The energy spectrum of Pope[10] is an excellent composite model for the entire wavenumber range and is used in this work.

The wavenumber spectrum of the structure function of pressure was examined successfully by Batchelor,[12] who showed that in the inertial range it falls off as $\kappa^{-7/3}$. Hill and Wilczak[13] use a different approach than Batchelor[12] but essentially confirm the result of Batchelor.[12] An additional insightful study by Gotoh and Rogallo[14] examined pressure statistics in homogeneous isotropic turbulence. Note that homogeneous isotropic turbulence velocity statistics are invariant under both translation and rotation. These theories played a role in the studies of wavenumber pressure spectra scaling in the atmosphere (see Albertson[15]) and within turbulent boundary layers (see Patwardhan and Ramesh[16]). The wavenumber pressure spectrum is incorporated into a composite function that is similar to that of Pope.[10]

The wavenumber temperature spectrum was initially considered successfully by Corrsin.[17,18] Corrsin[17] showed that the decay of the temperature spectrum is the same as the velocity spectrum in the inertial range. Lesieur et al.[19] and Lewalle[20] examined the decay of the variance of temperature in isotropic turbulence and also examined the decay of the wavenumber energy spectrum of temperature. Sreenivasan et al.[21] examined the intensity and decay of temperature variation of isotropic turbulence experimentally by examining flow behind grids of various shapes and at various Reynolds numbers. They also showed measurements from other researchers and collapsed their results.

Investigations of the wavenumber spectrum of density structure functions are rare. This is because of the difficulty of studying compressible turbulence with its associated high Reynolds number. The incompressible assumption is often used when studying other types of spectra. Nonetheless, Chandrasekhar[22] was likely the first to successfully consider density fluctuations in isotropic turbulence, at least insofar as the decay of intensity. Montgomery et al.,[23] who studied solar wind in the interstellar medium via magnetohydrodynamic turbulence, showed that a $\kappa^{-5/3}$ decay of the wavenumber density spectrum in the inertial range is likely.

It is generally accepted that wavenumber spectra possess self-similarity when the statistics are of low

order. In the initial period of decay or when the conditions of isotropic turbulence are not met, then similarity does not apply. Reid and Harris[24] presented these important points in relation to the initial period of decay, demonstrated similarity spectra of isotropic turbulence, and showed estimates of varying $E_u(\kappa)$. Ultimately, Reid and Harris[24] concluded that present theory is limited, and it is unfortunately necessary to resort to numerical methods to find the temporal and spatially evolving wavenumber spectra in the initial period of decay or when isotropy is not possible.

A number of theoretical (purely mathematical) approaches have been proposed to predict noise from isotropic turbulence. The first was created by Proudman[25] almost immediately after the development of the Lighthill[26–28] acoustic analogy. Proudman used the Lighthill acoustic analogy in conjunction with reductions of turbulent statistics for an isotropic turbulent field. Ultimately, Proudman[25] derived a scaling equation for the acoustic power, $P_a = \alpha\epsilon\mathcal{M}_t^5$, where α is a constant near unity, ϵ is the dissipation rate of turbulent kinetic energy, and M_t is the turbulent Mach number. Proudman[25] also showed that if the isotropic turbulence is undergoing decay then the acoustic power goes as $P_a = -(3/2)\alpha(\partial\overline{u}^2/\partial\tau)(\overline{u}^2c_\infty^{-2})^{5/2}$, where c_∞ is the ambient speed of sound, $\overline{u}$ is the root mean square fluctuation of one component of velocity, and τ is the retarded (source) time. The problem was not revisited until much later when Lilley[29,30] directly related the Lighthill stress tensor to the two-point cross-correlation function of isotropic turbulence. Lilley's effort yielded a closed-form mathematical model for the power spectral density of the acoustic pressure from isotropic turbulence, though only normalized spectra were compared with numerical results. Lilley[31] derived a similar formula by integrating the power spectrum of acoustic pressure and obtained $P_a = \alpha\rho_\infty u^8\mathcal{L}^{-1}c_\infty^{-5}$, where $\mathcal{L}$ is the characteristic length scale, and ρ_∞ is the ambient density. Lilley[31] demonstrated how his theory could be used for the prediction of noise from high speed jet flows. This is an astonishing accomplishment that convincingly showed how the theory of isotropic turbulence can predict the power spectrum of acoustic pressure from high Reynolds number turbulent jets.

The advent of digital computers has enabled the field of computational fluid dynamics (CFD) to be useful and has allowed numerical simulation of fluid turbulence. An extensive amount of research has been conducted, and here we will briefly survey important contributions of CFD related to isotropic turbulence because it plays a critical role in gaining insight into the dynamics of turbulent motions. Direct numerical simulation (DNS) of the Navier-Stokes equations attempts to fully resolve all scales of fluid turbulence. Typically, the Navier-Stokes equations are solved numerically and are restricted to relatively low Reynolds number because of the immense computational cost. Many efforts have been made to study homogeneous or isotropic turbulence using CFD. Notable examples include Passot and Pouquet,[32] who performed DNS of homogeneous turbulence, Mansour and Wray,[33] who examined low Reynolds number decaying turbulence (their results matched K41 and K62 theory), and Yao et al.,[34] who showed time correlations of pressure in an isotropic turbulent field (that are used here to partly validate the source model). Ishihara et al.[9] summarizes the state of the art in DNS.

The use of large eddy simulation (LES), which resolves relatively large scales of turbulence and either models the dynamics of the small scales or dissipates them implicitly (numerically), has also been used to study isotropic turbulence. Some important LES studies of isotropic turbulence include Langford and Moser,[35] who showed LES formulations for isotropic turbulence, Thornber et al.,[36] who used implicit LES to study decaying homogeneous turbulence, Vreman et al.,[37] who used a finite volume approach and attempted to quantify compressibility effects, and Abdibekov and Zhakebaev,[38] who studied decaying isotropic turbulence. Also, Hughes et al.[39] formulated various LES approaches for decaying, homogeneous isotropic turbulence; Zang et al.[40] performed LES of compressible isotropic turbulence, and Swanson et al.[41] studied decaying, homogeneous isotropic turbulence using various weighted essentially non-oscillatory (WENO) schemes and compared solutions with select theories. Both DNS and LES studies play a key role in the validation of the theory presented in this paper.

The sustained growth of digital computers has allowed numerical methods to be utilized to predict the noise from isotropic turbulence. The Lighthill[27] stress tensor can be directly approximated with the resolved time-varying field variables. One such approach is by Sarkar and Hussaini,[42] who performed DNS and used the Lighthill acoustic analogy to predict far-field acoustic pressure power spectra. It is not a coincidence that the successful numerical work of Sarkar and Hussaini[42] was conducted at the same time that Lilley[29] was visiting NASA Langley Research Center. Witkowska et al.[43] performed both LES and DNS on isotropic turbulence to study the possibility of using the approximate LES in place of DNS. In a similar study to Witkowska et al.,[43] Seror et al.[44] performed LES of stationary and decaying isotropic turbulence. Both Witkowska et al.[43] and Seror et al.[44] combined their approaches with the Lighthill acoustic analogy to

predict the radiating noise. An alternative numerical approach was proposed by Zhou and Dong,[45] who used a Lattice Boltzmann method in conjunction with the Lighthill acoustic analogy. The major advantage of numerical approaches is that they are essentially a 'numerical experiment,' if the governing equations are a representative model of fluid turbulence. As DNS resolves all scales of turbulence, then statistical quantities can be directly calculated. Unfortunately, the computational cost of numerical approaches restricts them to very low Reynolds numbers.

In this paper, we assume that the Navier-Stokes equations govern the dynamics of fluid turbulence. The Navier-Stokes equations are decomposed into a time evolving base flow, anisotropic fluctuations, isotropic fluctuations, radiating waves from anisotropic turbulence, and radiating waves from isotropic turbulence. The resulting equations possess a vector equivalent source that is equal to the Navier-Stokes equations operator on the base flow and turbulent fluctuating quantities. A linear Navier-Stokes equation operator results for the radiating waves and their anisotropic and isotropic associated components. We apply this model framework to statistically stationary and decaying isotropic turbulence. The isotropic base flow assumption allows for the vector Green's function of the linearized Navier-Stokes equations and energy equation to be found analytically. This vector Green's function is convolved with the equivalent sources. The density, pressure, temperature, and velocity are written as closed-form mathematical solutions. The power spectra of the field variables are then easily derived. A new unique method to approximate the vector equivalent source is proposed by relating it to the energy spectra of stationary and decaying isotropic turbulence. The remaining portion of this paper surveys the newly developed mathematical model. Select results are shown and are compared with DNS and acoustic power spectra from various sources.

Mathematical Theory

We assume that the Navier-Stokes equations govern the dynamics of fluid turbulence. The governing equations are the continuity equation

$$\frac{\partial \rho}{\partial t} + \frac{\partial \rho u_j}{\partial x_j} = 0, \tag{1}$$

momentum equation

$$\frac{\partial \rho u_i}{\partial t} + \frac{\partial \rho u_i u_j}{\partial x_j} = -\frac{\partial p}{\partial x_j}\delta_{ij} + \frac{\partial \tau_{ij}}{\partial x_j}, \tag{2}$$

and the energy equation

$$\frac{\partial \rho e_o}{\partial t} + \frac{\partial \rho u_j e_o}{\partial x_j} = -\frac{\partial u_j p}{\partial x_j} - \frac{\partial q_j}{\partial x_j} + \frac{\partial u_j \tau_{ij}}{\partial x_j}, \tag{3}$$

where e_o is the total energy per unit mass, p is the pressure, $\boldsymbol{u}$ is the velocity, t is the time, x is the spatial coordinate, and ρ is the density. Note that the use of Einstein notation implies summation. The shear stress is $\tau_{ij} = 2\mu S^*_{ij}$, where

$$S^*_{ij} = \frac{1}{2}\left(\frac{\partial u_i}{\partial x_j} + \frac{\partial u_j}{\partial x_i}\right) - \frac{1}{3}\frac{\partial u_k}{\partial x_k}\delta_{ij} \tag{4}$$

and δ_{ij} is the Kronecker delta function. Fourier's law provides the heat flux

$$q_j = -c_p \frac{\mu}{\mathcal{P}r}\frac{\partial T}{\partial x_j}, \tag{5}$$

where $\mathcal{P}r$ is the Prandtl number, $\mathcal{P}r = c_p \mu \lambda^{-1}$, and λ is the thermal conductivity. The total energy is related to the internal energy and kinetic energy as $e_o = e + u_k u_k/2$. The ideal gas equations are used and include $\gamma = c_p c_v^{-1}$, $p = \rho R T$, $e = c_v T$, and $R = c_p - c_v$. The unknown dependent variables are the density, velocity, pressure, and temperature, which are referred to here as the field variables. We decompose the field variables as

$$q = \overline{q} + \tilde{q} + \tilde{\tilde{q}} + q' + q'', \tag{6}$$

where q represents one of the field variables. The overbar operator represents the component of q that is the time-varying or time-averaged base flow. Tilde and double tilde operators represent the fluctuating component of turbulence that is characterized as anisotropic or isotropic, respectively, of the flow-field about the base flow. A single prime denotes the radiating component due to anisotropic turbulence. Likewise, the double prime denotes the radiating component due to isotropic turbulence. For example, pressure is decomposed as $p = \overline{p} + \tilde{p} + \tilde{\tilde{p}} + p' + p''$. The resulting equations are rearranged so that radiating quantities are on the left hand side, and the base flow and turbulent fluctuating quantities are on the right. We eliminate terms on the left hand side of the decomposed equations that are high order, because radiating quantities are much smaller than non-radiating quantities. The right hand sides are rearranged and result in the exact Navier-Stokes equations and energy equation operators working on the base flow and fluctuating turbulent quantities. The right hand sides are viewed as sources. The left hand sides are viewed as propagators. For example, the continuity equation can be written

$$\frac{\partial \overline{\rho} + \tilde{\rho} + \tilde{\tilde{\rho}} + \rho' + \rho''}{\partial t} + \frac{\partial}{\partial x_j}\left[\left(\overline{\rho} + \tilde{\rho} + \tilde{\tilde{\rho}} + \rho' + \rho''\right)\left(\overline{u}_j + \tilde{u}_j + \tilde{\tilde{u}}_j + u'_j + u''_j\right)\right] = 0. \tag{7}$$

We place non-radiating terms on the right hand side,

$$\begin{aligned}\frac{\partial\left(\rho' + \rho''\right)}{\partial t} + \frac{\partial}{\partial x_j}\left[\left(\rho' + \rho''\right)\left(\overline{u}_j + \tilde{u}_j + \tilde{\tilde{u}}_j\right) + \left(u'_j + u''_j\right)\left(\overline{\rho} + \tilde{\rho} + \tilde{\tilde{\rho}}\right) + \left(\rho' + \rho''\right)\left(u'_j + u''_j\right)\right] \\ = -\frac{\partial}{\partial t}\left(\overline{\rho} + \tilde{\rho} + \tilde{\tilde{\rho}}\right) - \frac{\partial}{\partial x_j}\left[\left(\overline{\rho} + \tilde{\rho} + \tilde{\tilde{\rho}}\right)\left(\overline{u}_j + \tilde{u}_j + \tilde{\tilde{u}}_j\right)\right]\end{aligned} \tag{8}$$

After performing these substitutions and rearranging we find the continuity source

$$\Theta_0 = -\frac{\partial \underline{\rho}}{\partial t} - \frac{\partial \underline{\rho}\underline{u}_j}{\partial x_j}, \tag{9}$$

the momentum sources are

$$\Theta_i = -\frac{\partial}{\partial t}\left[\underline{\rho}\underline{u}_i\right] - \frac{\partial}{\partial x_j}\left[\underline{\rho}\underline{u}_i\underline{u}_j\right] + \frac{\partial}{\partial x_j}\left\{\mu\left[\frac{\partial \underline{u}_i}{\partial x_j} + \frac{\partial \underline{u}_j}{\partial x_i}\right]\right\} - \frac{2}{3}\frac{\partial}{\partial x_j}\left\{\mu\frac{\partial}{\partial x_k}\underline{u}_k\right\} - \frac{\partial \underline{p}}{\partial x_j}\delta_{ij}, \tag{10}$$

for $i = 1$ to 3, and the energy source is

$$\begin{aligned}\Theta_4 = -\frac{\partial \underline{p}}{\partial t} - \frac{\gamma - 1}{2}\frac{\partial \underline{\rho}\underline{u}_k\underline{u}_k}{\partial t} - \gamma\frac{\partial \underline{u}_j\underline{p}}{\partial x_j} - \frac{\gamma - 1}{2}\frac{\partial \underline{\rho}\underline{u}_j\underline{u}_k\underline{u}_k}{\partial x_j} + (\gamma - 1)\frac{\partial}{\partial x_j}\left(\frac{c_p\mu}{\mathcal{P}r}\frac{\partial}{\partial x_j}\underline{T}\right) \\ + (\gamma - 1)\frac{\partial}{\partial x_j}\left[\mu\underline{u}_i\left(\frac{\partial \underline{u}_i}{\partial x_j} + \frac{\partial \underline{u}_j}{\partial x_i}\right)\right] - \frac{2}{3}\delta_{ij}\frac{\partial}{\partial x_j}\left[\mu\underline{u}_i\frac{\partial \underline{u}_k}{\partial x_k}\right].\end{aligned} \tag{11}$$

Here, the vector $\boldsymbol{\Theta} = \boldsymbol{\Theta}\left(\Theta_i\right)$, for $i = 0$ to 4, represents the right hand side. The underbar operator indicates the decomposition $\underline{q} = \overline{q} + \tilde{q} + \tilde{\tilde{q}}$, which applies to the aerodynamic variables. The vector term $\boldsymbol{\Theta}$ is very similar to the original governing equations. Because $\boldsymbol{\Theta}$ is the Navier-Stokes equations and energy equation operator, it might be assumed that it is zero. This is not the case as the radiating quantities have been removed; thus, it can also be viewed as a vector residual that is the source of sound. The sources are non-zero and are exactly the non-radiating component of the noise.

We now seek a statistical solution, assuming that a solution exists, and it has the form

$$q_k^{\perp}\left(\boldsymbol{x}, t\right) = \int_{-\infty}^{\infty} \ldots \int_{-\infty}^{\infty} \sum_{n=0}^{4} \boldsymbol{q}_{g,k}^{\perp n}\left(\boldsymbol{x}, t; \boldsymbol{y}, \tau\right)\Theta_n\left(\boldsymbol{y}, \tau\right) d\tau d\boldsymbol{y} \tag{12}$$

for $k = 0$ to 4, where $q_k^{\perp} = q'_k + q''_k$ and $q_{g,k}^{\perp} = q'_{g,k} + q''_{g,k}$. The vector $\boldsymbol{q}_{g,k}^{\perp,n} = \left[\rho_{g,k}^{\perp,n}, \boldsymbol{u}_{g,k}^{\perp,n}, p_{g,k}^{\perp,n}\right]^T$ satisfies a set of linear partial differential equations. The subscript g denotes the Green's function. This vector Green's function must obey conservation of mass

$$\frac{\partial \rho_g^{\perp n}}{\partial t} + \frac{\partial}{\partial x_j}\left[\rho_g^{\perp n}\underline{u}_j + u_{j,g}^{\perp n}\underline{\rho}\right] = \delta\left(\boldsymbol{x} - \boldsymbol{y}\right)\delta\left(t - \tau\right)\delta_{0n}, \tag{13}$$

conservation of momentum

$$\frac{\partial}{\partial t}\left[\rho_g^{\perp n}\underline{u}_i + u_{i,g}^{\perp n}\underline{\rho}\right] + \frac{\partial}{\partial x_j}\left[\rho_g^{\perp n}\underline{u}_i\underline{u}_j + u_{i,g}^{\perp n}\underline{\rho}\underline{u}_j + u_{j,g}^{\perp n}\underline{\rho}\underline{u}_i\right] - \overline{\mu}\frac{\partial}{\partial x_j}\left[\frac{\partial u_i^{\perp n}}{\partial x_j} + \frac{\partial u_j^{\perp n}}{\partial x_i}\right] + \frac{2}{3}\overline{\mu}\frac{\partial^2 u_k^{\perp n}}{\partial x_j \partial x_k} + \frac{\partial p^{\perp n}}{\partial x_j}\delta_{ij} = \delta\left(\boldsymbol{x}-\boldsymbol{y}\right)\delta\left(t-\tau\right)\delta_{in}, \tag{14}$$

and conservation of energy

$$\begin{aligned}
&\frac{\partial p^{\perp n}}{\partial t} + \frac{\gamma-1}{2}\frac{\partial}{\partial t}\left[\rho^{\perp n}\underline{u}_k^2 + 2u_k^{\perp n}\underline{\rho}\underline{u}_k\right] + \gamma\frac{\partial}{\partial x_j}\left[p^{\perp n}\underline{u}_j + u_j^{\perp n}\underline{p}\right] \\
&+\frac{\gamma-1}{2}\frac{\partial}{\partial x_j}\left[\rho^{\perp n}\underline{u}_j\underline{u}_k^2 + u_j^{\perp n}\underline{\rho}\underline{u}_k^2 + 2u_k^{\perp n}\underline{\rho}\underline{u}_k\right] - \frac{\partial}{\partial x_j}\frac{c_p\mu}{\mathcal{P}rR}\frac{\partial}{\partial x_j}\left[\frac{p'^n}{\rho'^n} + \frac{p''^n}{\rho''^n}\right] \\
&-\left(\gamma-1\right)\overline{\mu}\frac{\partial}{\partial x_j}\left[\underline{u}_i\left(\frac{\partial u_i^{\perp n}}{\partial x_j} + \frac{u_j^{\perp n}}{\partial x_i}\right) + u_i^{\perp n}\left(\frac{\underline{u}_i}{\partial x_j} + \frac{\underline{u}_j}{\partial x_i}\right)\right] \\
&+\frac{2}{3}\delta_{ij}\frac{\partial}{\partial x_j}\left[\mu\left(\underline{u}_i\right)\frac{\partial u_k^{\perp n}}{\partial x_k} + \mu\left(u_i^{\perp n}\right)\frac{\partial \underline{u}_k}{\partial x_k}\right] \\
&= \delta\left(\boldsymbol{x}-\boldsymbol{y}\right)\delta\left(t-\tau\right)\delta_{4n}
\end{aligned} \tag{15}$$

for viscosity $\mu \approx \overline{\mu}$. In addition, this set of equations satisfies q' and q'' in place of $q^{\perp}$.

We define the forward and inverse Fourier transforms as

$$\hat{\square}\left(f\right) = \int_{-\infty}^{\infty} \square \exp\left[-\omega i t\right] dt \quad \text{and} \quad \square\left(t\right) = \int_{-\infty}^{\infty} \hat{\square} \exp\left[\omega i t\right] df, \tag{16}$$

where the hat ($\hat{}$) operator signifies the Fourier transform, the $\square$ represents an argument, f is the frequency, $i = (-1)^{1/2}$, and $\omega = 2\pi f$. The forward Fourier transform of $q_{g,k}^{\perp j}\left(\boldsymbol{x},t;\boldsymbol{y},\tau\right)$ is

$$\hat{q}_{g,k}^{\perp j}\left(\boldsymbol{x};\boldsymbol{y},\omega\right) = \int_{-\infty}^{\infty} q_{g,k}^{\perp j}\left(\boldsymbol{x},t;\boldsymbol{y},\tau\right)\exp\left[-i\omega(t-\tau)\right] dt \tag{17}$$

and the inverse Fourier transform is

$$q_{g,k}^{\perp j}\left(\boldsymbol{x},t;\boldsymbol{y},\tau\right) = \frac{1}{2\pi}\int_{-\infty}^{\infty} \hat{q}_{g,k}^{\perp j}\left(\boldsymbol{x};\boldsymbol{y},\omega\right)\exp\left[i\omega(t-\tau)\right] d\omega. \tag{18}$$

Equation 12 can be rewritten using Eqs. 16 and 17 as

$$\hat{q}_k^{\perp}\left(\boldsymbol{x},\omega\right) = \int_{-\infty}^{\infty} \ldots \int_{-\infty}^{\infty} \sum_{j=0}^{4} q_{g,k}^{\perp j}\left(\boldsymbol{x},t;\boldsymbol{y},\tau\right)\Theta_j\left(\boldsymbol{y},\tau\right)\exp\left[-i\omega t\right] dt d\tau d\boldsymbol{y}. \tag{19}$$

Equation 19 represents the Fourier transform of $\boldsymbol{q}$ and is complicated by the fact that it contains both the retarded time, τ, and frequency, ω. We now seek to form the spectral density of $\boldsymbol{q}_k$. We assume that $q_k^{\perp}\left(\boldsymbol{x},t+\tau^{\dagger}\right)$ decays quickly near infinity so that its integral exists, which is reasonable given that it represents the vector Green's function. The superscript † denotes a particular retarded time, separate from τ, that is eventually eliminated. Also, we assume that the forward and inverse transforms of $q_k^{\perp}\left(\boldsymbol{x},t+\tau^{\dagger}\right)$ exist. We define the auto-correlation as

$$\left\langle q_k^{\perp}\left(\boldsymbol{x},\tau^{\dagger}\right) q_k^{\perp}\left(\boldsymbol{x},t+\tau^{\dagger}\right)\right\rangle = \lim_{T\to\infty}\frac{1}{2T}\int_{-T}^{T} q_k^{\perp *}\left(\boldsymbol{x},\tau^{\dagger}\right) q_k^{\perp}\left(\boldsymbol{x},t+\tau^{\dagger}\right) d\tau^{\dagger}. \tag{20}$$

Equation 20 can be written in an alternative form using the Wiener-Khinchin theory (see Wiener[46] for details), which states the auto-correlation is the Fourier transform of the absolute square of the Fourier

transform of $\boldsymbol{q}_k$. By using the Wiener-Khinchin theory in conjunction with the Fourier transform of $q_k^{\perp}$ and its complex conjugate, $q_k^{*\perp}$, an alternative integral equation for the auto-correlation can be formed.

We define the spectral density, S_k, as the inverse Fourier transform of the auto-correlation of the pressure

$$S_k^{\perp}(\boldsymbol{x},\omega) = \int_{-\infty}^{\infty} \left\langle q_k^{\perp}(\boldsymbol{x},t)\, q_k^{\perp}\left(\boldsymbol{x},t+\tau^{\dagger}\right)\right\rangle \exp\left[i\omega\tau^{\dagger}\right] d\tau^{\dagger}, \tag{21}$$

where $k = 0$ to 4 which corresponds to density, velocity components, and pressure, respectively. Using the general time-domain solution of Eq. 12 and the auto-correlation in the Wiener-Khinchin form, the spectral density of Eq. 21 is

$$\begin{aligned} S_k^{\perp}(\boldsymbol{x},\omega) = \int_{-\infty}^{\infty}\int_{-\infty}^{\infty} \Bigg[\int_{-\infty}^{\infty} \cdots \int_{-\infty}^{\infty} \sum_{m=0}^{4} q_{g,k}^{*\perp m}(\boldsymbol{x},t;\boldsymbol{y},\tau)\, \Theta_m(\boldsymbol{y},\tau) \exp[i\omega t]\, dt d\tau d\boldsymbol{y} \Bigg] \\ \times \Bigg[\int_{-\infty}^{\infty} \cdots \int_{-\infty}^{\infty} \sum_{n=0}^{4} q_{g,k}^{\perp n}(\boldsymbol{x},t';\boldsymbol{z},\tau')\, \Theta_n(\boldsymbol{z},\tau') \exp[-i\omega t']\, dt' d\tau' d\boldsymbol{z} \Bigg] \\ \times \exp\left[-i\omega\tau^{\dagger}\right] d\omega \exp\left[i\omega\tau^{\dagger}\right] d\tau^{\dagger}, \end{aligned} \tag{22}$$

where $\boldsymbol{z}$ denotes the second source position and the primes denote an alternative retarded time or observer time. We now integrate t and t', combine the resultant integrand within the inner summa, perform integration of ω and $\tau^{\dagger}$ (as they are the forward and inverse transforms and essentially result in a prefactor), and finally move terms within the integral involving τ. We obtain

$$\begin{aligned} S_k^{\perp}(\boldsymbol{x},\omega) = \int_{-\infty}^{\infty}\int_{-\infty}^{\infty}\int_{-\infty}^{\infty} \Bigg[\sum_{m=0}^{4}\sum_{n=0}^{4} \hat{q}_{g,k}^{*\perp m}(\boldsymbol{x};\boldsymbol{y},\omega)\, \hat{q}_{g,k}^{\perp n}(\boldsymbol{x};\boldsymbol{z},\omega) \\ \times \int_{-\infty}^{\infty} \Theta_m(\boldsymbol{y},\tau)\, \Theta_n(\boldsymbol{z},\tau')\, d\tau' \Bigg] d\tau d\boldsymbol{z} d\boldsymbol{y}. \end{aligned} \tag{23}$$

The vectors $\boldsymbol{y}$ and $\boldsymbol{z}$ and times τ and τ' are related through the equations $\boldsymbol{z} = \boldsymbol{y} + \boldsymbol{\eta}$ and $\tau' = \tau + \Delta\tau$. The spectral density is

$$\begin{aligned} S_k^{\perp}(\boldsymbol{x},\omega) = \int_{-\infty}^{\infty}\int_{-\infty}^{\infty}\int_{-\infty}^{\infty} \Bigg[\sum_{m=0}^{4}\sum_{n=0}^{4} \hat{q}_{g,k}^{*\perp m}(\boldsymbol{x};\boldsymbol{y},\omega)\, \hat{q}_{g,k}^{\perp n}(\boldsymbol{x};\boldsymbol{y}+\boldsymbol{\eta},\omega) \\ \times \int_{-\infty}^{\infty} \Theta_m(\boldsymbol{y},\tau)\, \Theta_n(\boldsymbol{y}+\boldsymbol{\eta},\tau+\Delta\tau)\, d\Delta\tau \Bigg] d\tau d\boldsymbol{\eta} d\boldsymbol{y}. \end{aligned} \tag{24}$$

The integrand involving retarded time is immediately recognizable as the two-point space-time cross-correlation between $\boldsymbol{\Theta}_m$ and $\boldsymbol{\Theta}_n$. Note that the source is a real function. We define $R_{m,n}(\boldsymbol{y},\boldsymbol{\eta},\tau)$ as the two-point space-time cross-correlation of the equivalent source

$$R_{m,n}^{\perp}(\boldsymbol{y},\boldsymbol{\eta},\tau) = \langle \Theta_m(\boldsymbol{y},\tau)\, \Theta_n(\boldsymbol{y}+\boldsymbol{\eta},\tau+\Delta\tau)\rangle = \int_{-\infty}^{\infty} \Theta_m(\boldsymbol{y},\tau)\, \Theta_n(\boldsymbol{y}+\boldsymbol{\eta},\tau+\Delta\tau)\, d\Delta\tau. \tag{25}$$

Using Eq. 25 we obtain the k^{th} spectral density

$$\boxed{S_k^{\perp}(\boldsymbol{x},\omega) = \int_{-\infty}^{\infty} \cdots \int_{-\infty}^{\infty} \sum_{m=0}^{4}\sum_{n=0}^{4} \hat{q}_{g,k}^{*\perp m}(\boldsymbol{x};\boldsymbol{y},\omega)\, \hat{q}_{g,k}^{\perp n}(\boldsymbol{x};\boldsymbol{y}+\boldsymbol{\eta},\omega)\, R_{m,n}^{\perp}(\boldsymbol{y},\boldsymbol{\eta},\tau)\, d\tau d\boldsymbol{\eta} d\boldsymbol{y}.} \tag{26}$$

Note that the integrand is dependent on the aerodynamic portion of the flow-field only. Equation 26 represents the k^{th} spectral density and is dependent on the two-point cross-correlation of the equivalent

sources ($R_{m,n}$) and the periodic vector Green's functions of the linearized Navier-Stokes equations and energy equation. The approach used herein implies

$$S_k^{\perp}(\boldsymbol{x},\omega) = S_k'(\boldsymbol{x},\omega) + S_k''(\boldsymbol{x},\omega) \tag{27}$$

and

$$R_{m,n}^{\perp} = R_{m,n}'(\boldsymbol{y},\boldsymbol{\eta},\tau) + R_{m,n}''(\boldsymbol{y},\boldsymbol{\eta},\tau). \tag{28}$$

Summation of spectral density is valid for linear acoustic problems. We do not consider the problem of nonlinear propagation here as it only occurs when extremely intense turbulent fields are present. The corresponding source terms, $R_{m,n}'$ and $R_{m,n}''$, must be independent because they correspond to linearly independent spectral densities. These relations can be substituted into Eq. 26 to independently predict the radiation from anisotropic or isotropic turbulence. Within this paper we use the latter substitution and focus on isotropic theory. The vector Green's function holds for all three forms of $S_k^{\perp}$, S_k', and S_k''. We seek to evaluate Eq. 26 using the theory of isotropic turbulence. This evaluation involves relating $R_{m,n}^{\perp}$ to the statistics of isotropic turbulence and finding an analytical solution of $q_{g,k}$. We first examine $R_{m,n}^{\perp}$.

Application to Isotropic Turbulence

We now adopt the assumptions and framework of a stationary or decaying isotropic turbulent field as originally introduced by Taylor[1] to the newly developed aeroacoustic theory. Using the decomposition of Eq. 6, the definition of the sources of Eqs. 9 through 11, and the definition of $R_{m,n}^{\perp}$ of Eq. 25, we can expand the two-point correlations of the base flow isotropic terms. For example, the continuity-continuity ($m = n$) two-point space time cross-correlation is

$$\begin{aligned} R_{0,0}^{\perp}(\boldsymbol{y},\boldsymbol{\eta},\tau) = &\left\langle \frac{\partial\tilde{\tilde{\rho}}^{(1)}}{\partial\tau}, \frac{\partial\tilde{\tilde{\rho}}^{(2)}}{\partial\tau} \right\rangle + 2\left\langle \frac{\partial\overline{\rho}^{(1)}\tilde{\tilde{u}}_j^{(1)} + \tilde{\tilde{\rho}}^{(1)}\tilde{\tilde{u}}_j^{(1)}}{\partial y_j}, \frac{\partial\tilde{\tilde{\rho}}^{(2)}}{\partial\tau} \right\rangle \\ &+ \left\langle \frac{\partial\overline{\rho}^{(1)}\tilde{\tilde{u}}_j^{(1)} + \tilde{\tilde{\rho}}^{(1)}\tilde{\tilde{u}}_j^{(1)}}{\partial y_j}, \frac{\partial\overline{\rho}^{(2)}\tilde{\tilde{u}}_m^{(2)} + \tilde{\tilde{\rho}}^{(2)}\tilde{\tilde{u}}_m^{(2)}}{\partial y_m} \right\rangle, \end{aligned} \tag{29}$$

where the superscript (1) or (2) signify that the quantity is evaluated at position $\boldsymbol{y}$ or $\boldsymbol{y}+\boldsymbol{\eta}$, respectively. Other terms of $R_{m,n}$ are shown in the appendix due to their large number of terms. The tensor $R_{m,n}$ can be calculated numerically using CFD either in the reduced form shown in the Appendix or in its original form shown in Eq. 25.

Here, we seek a more elegant method and approximate the terms using a newly developed approach. Each term ($<\square,\square>$) within $R_{m,n}$ can be written by its magnitude and associated two-point cross-correlation. The constant of each term is derived from the corresponding constant prefactor such as $\overline{\mu}$ or $\overline{\rho}$. The magnitude of the term is proportional to the fluctuating isotropic quantity divided by appropriate turbulence time or length scales. A new operation denoting magnitude ($<\widehat{\square}>$) of the fluctuating isotropic quantity is introduced and is dependent on the wavenumber, κ. Note each two-point cross-correlation for each cross-correlation term of $R_{m,n}$ is unique. We also assume that there is a steady base flow within the isotropic turbulent field, that is $\overline{\rho}$, $\overline{T}$, $\overline{p}$, etc., are constant. We propose the following general approximation for ($<\square,\square>$) of $R_{m,n}$

$$\left\langle \frac{\partial^{\mathcal{A},\mathcal{A}}\mathcal{C}_1 \spadesuit_A^{\blacktriangle,(1)} \clubsuit_{\mathcal{A}}^{\blacktriangledown,(1)}}{\partial\Gamma_{a,\alpha}}, \frac{\partial^{B,\mathcal{B}}\mathcal{C}_2 \heartsuit_B^{\blacksquare,(2)} \diamondsuit_{\mathcal{B}}^{\bigstar,(2)}}{\partial\gamma_{b,\beta}} \right\rangle \approx \mathcal{C}_1\mathcal{C}_2 \frac{\left\langle \widehat{\spadesuit_A^{\blacktriangle,(1)}} \right\rangle \left\langle \widehat{\clubsuit_{\mathcal{A}}^{\blacktriangledown,(1)}} \right\rangle}{\widehat{\langle\Gamma_{a,\alpha}\rangle}} \frac{\left\langle \widehat{\heartsuit_B^{\blacksquare,(2)}} \right\rangle \left\langle \widehat{\diamondsuit_{\mathcal{B}}^{\bigstar,(2)}} \right\rangle}{\widehat{\langle\gamma_{b,\beta}\rangle}} R_{\spadesuit\clubsuit\heartsuit\diamondsuit}. \tag{30}$$

Constants $\mathcal{C}_1$ and $\mathcal{C}_2$ are invariant to the cross-correlation and consist of terms such as γ, $\overline{\rho}$, $\overline{p}$, $\overline{T}$, $\overline{c}_p$, $\mathcal{P}_r$, $\overline{\mu}$, or δ_{ij}. Within the denominator, small case scripts a and α denote the i, j, and k indices of spatial derivatives. They are omitted if the derivative within the term is τ or if there is no second or first derivative. Likewise, small case scripts b and β correspond to l, m, and n indicial-spatial derivatives, and the same mapping rules apply. Recall that (1) or (2) denote that the value is dependent on the first or second point of the two-point cross-correlation, and in the context of homogeneous isotropic turbulence is invariant. The

suits represent fluctuating quantities $\tilde{\tilde{\rho}}$, $\tilde{\tilde{u}}$, $\tilde{\tilde{v}}$, $\tilde{\tilde{w}}$, $\tilde{\tilde{p}}$, or $\tilde{\tilde{T}}$, which correspond to the correlation being examined. Within the numerator the $\partial^{A,\mathcal{A}}$ represents the order of the spatial or temporal partial derivative, correspond to a and α, respectively, and is partially omitted if the partial derivative is of first order or entirely omitted if the partial derivative is of zeroth order. Many terms involve summation over repeated indices, and these are reflected when $A = a$, $\mathcal{A} = \alpha$, $B = b$, or $\mathcal{B} = \beta$. Within the denominator, Γ and γ are either y or τ or omitted if a partial derivative is not acting on a suit. Darkened symbols ▲, ▼, ■, and ★, represent powers of the fluctuating quantity. The magnitude operation on a spatial derivative ($< \widehat{\partial y_i} >$) results in $l(\kappa)$ (turbulent length scale at wavenumber κ in the direction of the spatial derivative). Likewise, ($< \widehat{\partial \tau} >$) results in $\tau(\kappa)$, which is the turbulent time scale at wavenumber κ. The $< \widehat{\square} >$ operator on the field variables is proportional to the field variable's 'energy' at κ, and we discuss this relation later. We write the normalized two-point cross-correlations as a vector $\boldsymbol{R} = R_{\spadesuit\clubsuit\heartsuit\diamondsuit} + ...$, and assume that it has a single universal form.

We now illustrate the mapping of Eq. 30 with an example. For example, the second term of $R^{\perp}_{0,0}(\boldsymbol{y}, \boldsymbol{\eta}, \tau)$ results in

$$2\left\langle \frac{\partial \overline{\rho}^{(1)} \tilde{\tilde{u}}_j^{(1)} + \tilde{\tilde{\rho}}^{(1)} \tilde{\tilde{u}}_j^{(1)}}{\partial y_j}, \frac{\partial \tilde{\tilde{\rho}}^{(2)}}{\partial \tau} \right\rangle \approx 6 \left\{ \overline{\rho} \frac{\widehat{\langle \tilde{\tilde{\rho}} \rangle \langle \tilde{\tilde{u}} \rangle}}{l\tau} + \frac{\widehat{\langle \tilde{\tilde{\rho}} \rangle^2 \langle \tilde{\tilde{u}} \rangle}}{l\tau} \right\} \boldsymbol{R}. \tag{31}$$

We now use Eq. 30 on all terms of $R_{m,n}$. The continuity-continuity two-point cross-correlation is

$$R^{\perp}_{0,0}(\boldsymbol{y}, \boldsymbol{\eta}, \tau) \approx \left\{ \left(-\frac{\overline{\rho} + \widehat{\langle \tilde{\tilde{\rho}} \rangle}}{\tau} - \frac{3\widehat{\langle \tilde{\tilde{u}} \rangle} \left(\overline{\rho} + \widehat{\langle \tilde{\tilde{\rho}} \rangle} \right)}{l} \right)^2 \right\} \boldsymbol{R}, \tag{32}$$

the continuity-momentum two-point cross-correlation is

$$\begin{aligned} R^{\perp}_{0,l}(\boldsymbol{y}, \boldsymbol{\eta}, \tau) \approx \Bigg\{ & \left(-\frac{3\left(\overline{\rho} + \widehat{\langle \tilde{\tilde{\rho}} \rangle} \right) \widehat{\langle \tilde{\tilde{u}} \rangle}}{l} - \frac{\left(\overline{\rho} + \widehat{\langle \tilde{\tilde{\rho}} \rangle} \right)}{\tau} \right) \\ & \times \left(-\frac{\widehat{\langle \tilde{\tilde{p}} \rangle}}{l} + \frac{4\widehat{\langle \tilde{\tilde{u}} \rangle} \overline{\mu}}{l^2} - \frac{3\left(\overline{\rho} + \widehat{\langle \tilde{\tilde{\rho}} \rangle} \right) \widehat{\langle \tilde{\tilde{u}} \rangle}^2}{l} - \frac{\left(\overline{\rho} + \widehat{\langle \tilde{\tilde{\rho}} \rangle} \right) \widehat{\langle \tilde{\tilde{u}} \rangle}}{\tau} \right) \Bigg\} \boldsymbol{R}, \end{aligned} \tag{33}$$

the continuity-energy two-point cross-correlation is

$$\begin{aligned} R^{\perp}_{0,4}(\boldsymbol{y}, \boldsymbol{\eta}, \tau) \approx \Bigg\{ & \left(-\frac{3\left(\overline{\rho} + \widehat{\langle \tilde{\tilde{\rho}} \rangle} \right) \widehat{\langle \tilde{\tilde{u}} \rangle}}{l} - \frac{\left(\overline{\rho} + \widehat{\langle \tilde{\tilde{\rho}} \rangle} \right)}{\tau} \right) \left(-\frac{3\gamma \widehat{\langle \tilde{\tilde{u}} \rangle} \left(\overline{\rho} + \widehat{\langle \tilde{\tilde{p}} \rangle} \right)}{l} - \frac{6\overline{\mu} \widehat{\langle \tilde{\tilde{u}} \rangle}^2}{l^2} + \frac{3c_p \widehat{\left\langle \tilde{\tilde{T}} \right\rangle} (\gamma - 1) \overline{\mu}}{Prl^2} \right. \\ & \left. + \frac{9\overline{\mu} (\gamma - 1) \widehat{\langle \tilde{\tilde{u}} \rangle}^2}{l^2} - \frac{9(\gamma - 1) \left(\overline{\rho} + \widehat{\langle \tilde{\tilde{\rho}} \rangle} \right) \widehat{\langle \tilde{\tilde{u}} \rangle}^3}{2l} - \frac{\widehat{\langle \tilde{\tilde{p}} \rangle}}{\tau} - \frac{3(\gamma - 1) \left(\overline{\rho} + \widehat{\langle \tilde{\tilde{\rho}} \rangle} \right) \widehat{\langle \tilde{\tilde{u}} \rangle}^2}{2\tau} \right) \Bigg\} \boldsymbol{R}, \end{aligned} \tag{34}$$

the momentum-momentum two-point cross-correlation is

$$R^{\perp}_{i,l}(\boldsymbol{y}, \boldsymbol{\eta}, \tau) \approx \left\{ \left(-\frac{\widehat{\langle \tilde{\tilde{p}} \rangle}}{l} + \frac{4\overline{\mu} \widehat{\langle \tilde{\tilde{u}} \rangle}}{l^2} - \frac{3\left(\overline{\rho} + \widehat{\langle \tilde{\tilde{\rho}} \rangle} \right) \widehat{\langle \tilde{\tilde{u}} \rangle}^2}{l} - \frac{\left(\overline{\rho} + \widehat{\langle \tilde{\tilde{\rho}} \rangle} \right) \widehat{\langle \tilde{\tilde{u}} \rangle}}{\tau} \right)^2 \right\} \boldsymbol{R}, \tag{35}$$

the momentum-energy two-point cross-correlation is

$$R_{i,4}^{\perp}\left(\boldsymbol{y},\boldsymbol{\eta},\tau\right)\approx\left\{\left(-\frac{\widehat{\langle\tilde{\bar{p}}\rangle}}{l}+\frac{4\overline{\mu}\widehat{\langle\tilde{\bar{u}}\rangle}}{l^2}-\frac{3\left(\overline{\rho}+\widehat{\langle\tilde{\bar{\rho}}\rangle}\right)\widehat{\langle\tilde{\bar{u}}\rangle}^2}{l}-\frac{\left(\overline{\rho}+\widehat{\langle\tilde{\bar{\rho}}\rangle}\right)\widehat{\langle\tilde{\bar{u}}\rangle}}{\tau}\right)\right.$$
$$\times\left(-\frac{3\gamma\left(\overline{p}+\widehat{\langle\tilde{\bar{p}}\rangle}\right)\widehat{\langle\tilde{\bar{u}}\rangle}}{l}-\frac{6\overline{\mu}\widehat{\langle\tilde{\bar{u}}\rangle}^2}{l^2}+\frac{3c_p\overline{\mu}\left(\gamma-1\right)\widehat{\left\langle\tilde{\bar{T}}\right\rangle}}{Prl^2}+\frac{9\left(\gamma-1\right)\overline{\mu}\widehat{\langle\tilde{\bar{u}}\rangle}^2}{l^2}\right.$$
$$\left.\left.-\frac{9\left(\gamma-1\right)\left(\overline{\rho}+\widehat{\langle\tilde{\bar{\rho}}\rangle}\right)\widehat{\langle\tilde{\bar{u}}\rangle}^3}{2l}-\frac{\widehat{\langle\tilde{\bar{p}}\rangle}}{\tau}-\frac{3\left(\gamma-1\right)\left(\overline{\rho}+\widehat{\langle\tilde{\bar{\rho}}\rangle}\right)\widehat{\langle\tilde{\bar{u}}\rangle}^2}{2\tau}\right)\right\}\boldsymbol{R},\tag{36}$$

and finally, the energy-energy two-point cross-correlation is

$$R_{4,4}^{\perp}\left(\boldsymbol{y},\boldsymbol{\eta},\tau\right)\approx\left\{\left(-\frac{3\gamma\widehat{\langle\tilde{\bar{u}}\rangle}\left(\overline{p}+\widehat{\langle\tilde{\bar{p}}\rangle}\right)}{l}-\frac{6\overline{\mu}\widehat{\langle\tilde{\bar{u}}\rangle}^2}{l^2}+\frac{3c_p\overline{\mu}\left(\gamma-1\right)\widehat{\left\langle\tilde{\bar{T}}\right\rangle}}{Prl^2}+\frac{9\left(\gamma-1\right)\overline{\mu}\widehat{\langle\tilde{\bar{u}}\rangle}^2}{l^2}\right.\right.$$
$$\left.\left.-\frac{9\left(\gamma-1\right)\left(\overline{\rho}+\widehat{\langle\tilde{\bar{\rho}}\rangle}\right)\widehat{\langle\tilde{\bar{u}}\rangle}^3}{2l}-\frac{\widehat{\langle\tilde{\bar{p}}\rangle}}{\tau}-\frac{3\left(\gamma-1\right)\left(\overline{\rho}+\widehat{\langle\tilde{\bar{\rho}}\rangle}\right)\widehat{\langle\tilde{\bar{u}}\rangle}^2}{2\tau}\right)^2\right\}\boldsymbol{R}.\tag{37}$$

Let

$$R_{m,n}^{\perp}\left(\boldsymbol{y},\boldsymbol{\eta},\tau\right)=\left\{R_{m,n}^{\perp}\right\}\boldsymbol{R},\tag{38}$$

where $R_{m,n}$ are the bracketed terms of Eqs. 32 through 37. We now require a model for $\boldsymbol{R}$, and (for simplicity) we assume that it has a universal form. The vector $\boldsymbol{R}$ is unique for each combination of m and n. It is not practical to create an analytical model for each term within Eqs. 32 through 37. These correlations could be calculated numerically for specific turbulent fields. However, on a practical basis each normalized two-point cross-correlation has some identifying features such as being unity at zero time delay and zero separation, decaying to zero for very large spatial separations or time delays, and a transition from exponentially decaying to Gaussian decaying statistics. We propose a simplified universal form of the two-point normalized cross-correlation

$$\boldsymbol{R}\approx\exp\left[-\left(\frac{\iota_c\eta_i^2}{l_i^2}+\frac{\left(1-\iota_c\right)\left|\eta_i\right|}{l_i}\right)-c_{\kappa l}^2\kappa^2\eta_i^2\right]\exp\left[-\left(\frac{\iota_c\Delta\tau^2}{\tau^2}+\frac{\left(1-\iota_c\right)\left|\Delta\tau\right|}{\tau}\right)-c_{\kappa\tau}^2\kappa^2u_s^2\Delta\tau^2\right],\tag{39}$$

where ι_c is a real-valued constant bounded from zero to one. Equation 39 exhibits Gaussian statistics for $\iota_c=1$ and exhibits exponentially decaying statistics for $\iota_c=0$. A mixed Gaussian-exponentially decaying model results when $0<\iota_c<1$. The validation and choice of ι_c will be explored in a later section. We substitute Eq. 38 into the model Eq. 26 and isolate integrals involving $\boldsymbol{\eta}_i$ and $\Delta\tau$. These integrals are evaluated analytically

$$\int_{-\infty}^{\infty}\int_{-\infty}^{\infty}\boldsymbol{R}\,d\tau d\boldsymbol{\eta}=\pi^2\left[\left(l_1^{-2}+c_{\kappa l}^2\kappa^2\right)\left(l_2^{-2}+c_{\kappa l}^2\kappa^2\right)\left(l_3^{-2}+c_{\kappa l}^2\kappa^2\right)\left(c_{\kappa\tau}^2u^2\kappa^2+\tau^{-2}\right)\right]^{-1/2},\tag{40}$$

assuming that $l>0$, $\tau>0$, $u>0$, and are real. We set the constant coefficients $c_{\kappa\tau}$ and $c_{\kappa l}$ to zero for simplicity, but these could be adjusted to capture trends in measurement more accurately. We now relate the $\widehat{\langle\square_i\rangle}$ operator on the field variable to energy spectra. Let

$$\widehat{\langle\tilde{\bar{u}}_i\rangle}\left(\boldsymbol{y},\tau\right)=\sqrt{\frac{2}{3}}\left(\int_{\kappa_1}^{\kappa_2}E_u(\boldsymbol{y},\kappa,\tau)d\kappa\right)^{1/2},\tag{41}$$

$$\widehat{\left\langle \tilde{\tilde{\rho}} \right\rangle}(\boldsymbol{y},\tau) = \left(\int_{\kappa_1}^{\kappa_2} E_\rho(\boldsymbol{y},\kappa,\tau) d\kappa \right)^{1/2}, \tag{42}$$

$$\widehat{\left\langle \tilde{\tilde{p}} \right\rangle}(\boldsymbol{y},\tau) = \left(\int_{\kappa_1}^{\kappa_2} E_p(\boldsymbol{y},\kappa,\tau) d\kappa \right)^{1/2}, \tag{43}$$

and,

$$\widehat{\left\langle \tilde{\tilde{T}} \right\rangle}(\boldsymbol{y},\tau) = \left(\int_{\kappa_1}^{\kappa_2} E_T(\boldsymbol{y},\kappa,\tau) d\kappa \right)^{1/2}, \tag{44}$$

where E_u, E_ρ, E_p, and E_T are the 'energy' spectra of the difference functions of the field variables, and κ_1 and κ_2 are the limits of integration. Limits of integration are selected for unit bandwidth predictions, that is $\kappa_2 - \kappa_1 = 2\pi c_\infty^{-1}$ because $\omega = 2\pi f = c_\infty \kappa$. For statistically stationary isotropic turbulence the spectra are invariant with time and for decaying isotropic turbulence are dependent on τ. The turbulent kinetic energy is related to the wavenumber energy spectrum

$$k_u = \frac{1}{2} < u_i u_i > = \int_0^\infty E_u(\kappa,t) d\kappa \tag{45}$$

and the dissipation of turbulent kinetic energy is

$$\epsilon_u = 2\nu \int_0^\infty \kappa^2 E_u(\kappa,t) d\kappa. \tag{46}$$

Wavenumber Spectra

We now define the wavenumber spectra to close the model for S_k. The wavenumber spectra represent a small set of exact analytical results within the field of statistical fluid mechanics. Unfortunately, the theory is not complete, and we must resort to some physical arguments to close particular portions. The energy spectrum of u is

$$E_u(\kappa,\tau) = \frac{1}{2\pi^3} \int_{-\infty}^{\infty} \int_{-\infty}^{\infty} \int_{-\infty}^{\infty} \langle u_i(\boldsymbol{t},\tau) u_j(\boldsymbol{y}+\boldsymbol{r},\tau) \rangle \exp\left[-i\boldsymbol{\kappa}\cdot\boldsymbol{r}\right] d^3\boldsymbol{r}, \tag{47}$$

where $\boldsymbol{r}$ is a separation vector between two points within the isotropic field. We adopt the spectrum for $E_u(\kappa)$ based on the work of Kolmogorov[2–4,11]

$$E_u(\kappa) = c_u \epsilon^{2/3} \kappa^{-5/3} f_{L,u}(\kappa L) f_{\eta,u}(\kappa\eta), \tag{48}$$

where $c_u = 1.5$ is a constant, L is the integral length scale, and η is the Kolmogorov[2–4,11] length scale. We have included functions f_L and f_η, defined by Pope,[10] so that E_u represents a composite spectrum (for all κ). These latter functions are shown following other definitions of energy spectra. Batchelor[12] showed that the pressure correlation is a function of the fourth order moment of turbulent velocity, and this relation is written as

$$E_p(\kappa) = \frac{1}{8\pi^2} \int_{-\infty}^{\infty} \int_{-\infty}^{\infty} \int_{-\infty}^{\infty} E_u(\kappa^{(2)}) E_u(|\boldsymbol{\kappa}^{(1)} - \boldsymbol{\kappa}^{(2)}|) \frac{\sin^4\theta}{|\boldsymbol{\kappa}^{(1)} - \boldsymbol{\kappa}^{(2)}|^4} d\tau(\boldsymbol{\kappa}^{(2)}). \tag{49}$$

Batchelor[12] shows that within the inertial range the variation of the wavenumber spectrum of p goes as $\kappa^{-7/3}$. We adopt the pressure spectrum derived by Gotoh and Rogallo[14] and multiply by functions $f_{L,p}(\kappa L)$ and $f_{\eta,p}(\kappa\eta)$ and obtain

$$E_p(\kappa) = c_p \epsilon^{4/3} \kappa^{-7/3} f_{L,p}(\kappa L) f_{\eta,p}(\kappa\eta), \tag{50}$$

where c_p is a constant and set to unity. The decay of temperature fluctuations and the spectrum of E_T were investigated by Corrsin,[17,18] and based upon Corrsin's investigation we define

$$E_T(\kappa, t) = c_T \epsilon^{1/3} \kappa^{-5/3} f_{L,T}(\kappa L) f_{T,\eta}(\kappa\eta), \tag{51}$$

where c_T is a constant and set to unity.

Montgomery et al.[23] used the theory of Batchelor[12] and found a particular density-pressure equation of state. An omnidirectional spectrum is formed through multiplication by $4\pi\kappa^2$. A relation similar to Eq. 49 is formed, and Montgomery et al.[23] show that E_ρ possesses a $\kappa^{-5/3}$ fall-off within the inertial range. Based on this limited knowledge of the spectrum of E_ρ, we propose a composite spectrum

$$E_\rho(\kappa) = c_\rho \epsilon^{1/7} \kappa^{-5/3} f_{L,\rho}(\kappa L) f_{\eta,\rho}(\kappa\eta), \tag{52}$$

where c_ρ is a constant and set to unity.

Unlike the coefficient c_u, the coefficients, c_p, c_T, and c_ρ, are unknown to the community. Unfortunately, finding values of these coefficients analytically is a difficult task that has yet to be accomplished. They are likely on the same order of magnitude as c_u. If they were orders of magnitude larger or smaller then the noise predictions would be much too high or low, respectively. These coefficients are very insensitive on the predicted noise spectrum compared to the powers of ϵ and κ.

Spectra defined in Eqs. 48, 50, 51, and 52 contain composite functions f_{Li} and $f_{\eta i}$. Though they are likely unique in nature, especially with regard to their power as they are functions of κ, we approximate them as a single function $f_L \approx f_{Li}$ and $f_\eta \approx f_{\eta i}$. Functions f_L and f_η are unity throughout the inertial range and are positive values less than unity at low or high wavenumbers. This approach allows for a complete and continuous composite spectrum to be constructed. The functions f_L and f_η are adopted from Pope[10] and calibrated against numerically predicted E_u of stationary DNS at multiple $\mathcal{R}e$ to handle low and high wavenumber regions. The functions f_L and f_η are

$$f_L(\kappa L) = \left[\frac{\kappa L}{[(\kappa L)^2 + c_L]^{1/2}} \right]^{5/3+p_o}, \tag{53}$$

where $p_o = 2$ is a constant and

$$f_\eta(\kappa\eta) = \exp\left[-\beta \left\{ \left[(\kappa\eta)^4 + c_\eta^4 \right]^{1/4} - c_\eta \right\} \right], \tag{54}$$

where $\beta = 2.1$ is a constant. The constants c_L and c_η are calculated by using the definition of Eqs. 45 and 46 and are approximately 6.78 and 0.40, respectively. We now model the dynamics of the scales of turbulence for stationary and decaying isotropic turbulence. Let

$$\mathcal{R}e_t = \frac{k^2}{\epsilon\nu} = \frac{k^{1/2} L}{\nu}, \tag{55}$$

be the turbulent Reynolds number, where ν is the kinematic viscosity.

Recall that L is the integral length scale, and for simplicity we approximate the integral length scale with the characteristic length scale $\mathcal{L}$, that is $L \approx \mathcal{L}$. The range of turbulent length scales is $\alpha_1 l_\eta \lessapprox l \lessapprox \alpha_2 l_o$, where $\kappa = 2\pi l^{-1}$. It is generally accepted that the constants α_1 and α_2 are approximately 0.15 and 6, respectively (see Pope[10]). The Kolmogorov length scale is $\eta = \mathcal{L}\mathcal{R}e_t^{-3/4}$. The range of wavenumbers is restricted to $\alpha_1\kappa_\eta \gtrapprox \kappa \gtrapprox \alpha_2\kappa_o$. The velocity scale is then estimated as

$$u = (\epsilon l)^{1/3} \tag{56}$$

and the time scale as

$$\tau = \left(\frac{l^2}{\epsilon} \right)^{1/3}. \tag{57}$$

Wavenumber Spectra Dynamics

Thus far, the developed equations are sufficient to predict the noise from stationary isotropic turbulence. For decaying isotropic turbulence, additional models are required to characterize the evolving wavenumber spectra and turbulent scales. We model the variation of the wavenumber spectra through the statistics of the time-evolving turbulent scales. We assume that initially the turbulence is fully developed and stationary (that production is equal to dissipation) and at some instant of time, the turbulence starts decaying. In decaying isotropic turbulence that is initially fully developed, there is no production, thus

$$\frac{\partial k}{\partial \tau} = -\epsilon. \tag{58}$$

The variation of length scales within decaying isotropic turbulence was investigated by Lesieur et al.,[19] who showed that the length scale l_u is modeled approximately by

$$\frac{1}{2}\frac{\partial}{\partial \tau} l_u^2 \approx \epsilon^{1/3} l_u^{4/3}. \tag{59}$$

Unfortunately, the closed-form solution of this nonlinear partial differential equation is unknown as ϵ is dependent on τ. Lesieur et al.[19] observed in measurement that l_u decays approximately as $l_u \propto \tau^{0.31}$. Thus, we propose

$$l \approx l_o(1 + \tau^{0.31}), \tag{60}$$

where l_o is an initial length scale at initial wavenumber κ_o at $\tau = \tau_o$.

Batchelor[12] examined the variation of the statistics associated with pressure and approximates $\langle p^2 \rangle \approx 0.34\overline{\rho}^2 \langle u^2 \rangle^2$. Based on Yao et al.,[34] we propose that the decay of pressure fluctuations is proportional to k, $\langle pp \rangle (\tau) \propto k(\tau)$, and $l_p \propto l_u$. Corrsin[17,18] investigated the decay of $\langle TT' \rangle$ within a decaying isotropic field and argued

$$\frac{\partial \langle TT' \rangle}{\partial t} = -12\gamma \frac{\langle TT' \rangle}{\lambda_T^2}, \tag{61}$$

where λ_T is the Taylor microscale of temperature (see Corrsin[17,18] for details) and the approximate model solution is

$$\langle TT' \rangle \propto \exp\left[-\frac{r^2}{8\gamma\tau}\right] (\gamma\tau)^{-3/2}. \tag{62}$$

Another form of the solution was proposed by Lesieur et al.,[19] who argued that the integral scale of temperature is proportional to the integral scale of velocity, $l_T(\tau) \propto l_u(\tau)$, as they are governed by a similar differential equation with the same power coefficients. Unfortunately, very little is known about the dynamics of the statistics involving density, but Montgomery et al.[23] imply that they are very likely similar to those of pressure.

Due to the lack of knowledge regarding the variation of turbulent statistics and length scales of decaying isotropic turbulence, we do not develop closed-form explicit equations for their variation with time. Instead we simulate their decay by assuming an initial stationary isotropic field decays from time τ_o to sometime τ, where the subscript o is the initialization time ($\tau_o > 0$). At each time τ, a series of equations are evaluated in order of their dependence that are used in turn to calculate the spectra, E_q.

First, at given time τ, $L_{c,o}$ and $\mathcal{R}_{t,o}$ are known and the integral length scale is estimated using Eq. 60. Then the turbulent kinetic energy within the system is estimated using $k = k_o - \int_{\tau_o}^{\tau} \epsilon d\tau$. Evaluation of this integral requires knowledge of ϵ between τ_o and τ. The turbulent Reynolds number, $\mathcal{R}e_t = k^{1/2} L \nu_\infty^{-1}$, dissipation, $\epsilon = k^2 \mathcal{R}e_t \nu_\infty^{-1}$, and Kolmogorov length scale, $\eta = L\mathcal{R}e_t^{-3/4}$, are then calculated. Limits of integration for E_q at time τ are estimated as $\kappa_{min} = \pi L^{-1}/50$ and $\kappa_{max} = 20\pi\eta^{-1}$. Finally, the Taylor length scale, $\lambda = 10^{1/2} L \mathcal{R}e_t^{-1/2}$, and Taylor Reynolds number, $\mathcal{R}e_\lambda = \sqrt{2k/3}\lambda\nu_\infty^{-1}$, are calculated. It is emphasized that these equations are found iteratively, and their arguments are dependent on the previous iteration. We will examine the validity of predicting decaying turbulent statistics using this approach within the results section.

Vector Green's Function for Homogeneous Isotropic Turbulence

Arguments have been proposed for the source term within model Eq. 26. Here, we derive the necessary vector Green's function to evaluate Eq. 26 for $k = 4$ (spectral density of acoustic pressure) given the assumptions of homogeneous isotropic turbulence or homogeneous decaying isotropic turbulence. We assume that the environment is quiescent except for a region of homogeneous, decaying or stationary, isotropic turbulence. Note that the Green's function for $q^{\perp}$ is the same as for q' and q'', where $q^{\perp} = q' + q''$. We assume that the viscosity is constant, $\mu \approx \overline{\mu}$, and does not play an important role in the propagation of sound (see Lighthill[47]). The vector Green's function $q^{\perp}$ is governed by Eqs. 13, 14, and 15. Using these assumptions, we take the partial time derivative of the energy equation and use the relation $\overline{c}^2\overline{\rho} = \overline{\gamma p}$ and obtain

$$\frac{\partial^2 p_g^{\perp n}}{\partial t^2} + \overline{c}^2\overline{\rho}\frac{\partial^2 u_{j,g}^{\perp n}}{\partial t \partial x_j} = \frac{\partial}{\partial t}\left[\delta\left(\boldsymbol{x}-\boldsymbol{y}\right)\delta\left(t-\tau\right)\delta_{4n}\right]. \tag{63}$$

The partial derivative $\partial/\partial x_i$ is applied to the momentum Green's function. The result is multiplied by $\overline{c}^2$, and we obtain

$$\overline{c}^2\overline{\rho}\frac{\partial^2 u_{i,g}^{\perp n}}{\partial x_i \partial t} + \overline{c}^2\frac{\partial^2 p_g^{\perp n}}{\partial x_i \partial x_j}\delta_{ij} = \overline{c}^2\frac{\partial}{\partial x_i}\left[\delta\left(\boldsymbol{x}-\boldsymbol{y}\right)\delta\left(t-\tau\right)\delta_{in}\right]. \tag{64}$$

Equation 64, for $i = 1$, 2, and 3 is subtracted from Eq. 63. The resulting equation is written in spherical coordinates then simplified with the identity $\delta(\boldsymbol{x}) = \delta(x)\delta(y)\delta(z)$. The Fourier transform of the resulting equation is performed. Finally, the Fourier transforms of δ is unity and $\partial\delta/\partial t$ is $-i\omega$ are used. The result is

$$\begin{aligned} -\omega^2\hat{p}_g^{\perp n} - \overline{c}^2\left[\frac{1}{r^2}\frac{\partial}{\partial r}\left[r^2\frac{\partial \hat{p}_g^{\perp n}}{\partial r}\right] + \frac{1}{r^2\sin[\theta]}\frac{\partial}{\partial\theta}\left(\sin[\theta]\frac{\partial \hat{p}_g^{\perp n}}{\partial \phi^2}\right) + \frac{1}{r^2\sin^2[\theta]}\frac{\partial^2 \hat{p}_g^{\perp n}}{\partial \phi^2}\right] \\ = -i\omega\delta(r\sin[\theta]\cos[\phi])\delta(r\sin[\theta]\sin[\phi])\delta(r\cos[\theta])\delta_{4n} \\ -\overline{c}^2\frac{\partial}{\partial x_j}\left[\delta(r\sin[\theta]\cos[\phi])\delta(r\sin[\theta]\sin[\phi])\delta(r\cos[\theta])\delta_{jn}\right]. \end{aligned} \tag{65}$$

We seek solutions of Eq. 65 that have unique right hand sides for cases $n = 1$ through 4. The right hand side of Eq. 65 for $n = 0$ is 0, for $n = 1$ to 3 is $-\overline{c}^2\partial r^2\delta(r)/\partial r\delta_{jn}$, and for $n = 4$ is $-i\omega\delta(r)$. We first seek a solution of Eq. 65 with the right hand side corresponding to $n = 4$. As the medium through which the waves propagate is quiescent, it is expected that a point source for the $n = 4$ case will be symmetric. The symmetric solution will contain no variation with respect to θ and ϕ and now Eq. 65 becomes

$$-\omega^2\hat{p}_g^{\perp,(4)} - \frac{\overline{c}^2}{r^2}\frac{\partial}{\partial r}\left[r^2\frac{\partial \hat{p}_g^{\perp,(4)}}{\partial r}\right] = -i\omega\delta(r). \tag{66}$$

The solution is

$$\hat{p}_g^{\perp,(4)} = c_1\frac{\exp\left[-r\sqrt{\frac{-\omega^2}{\overline{c}^2}}\right]}{r} + c_2\frac{\exp\left[r\sqrt{\frac{-\omega^2}{\overline{c}^2}}\right]}{r\sqrt{\frac{-\omega^2}{\overline{c}^2}}}, \tag{67}$$

where c_1 and c_2 are constants. We have not made any assumptions regarding the properties of ω or $\overline{c}$. The solution of Eq. 65 for $n = 0$ is trivial because it is a homogeneous wave equation for $p_g^{\perp 0}$. Solution of Eq. 65 for $n = 1$ to 3 is also simple if the right hand side is written in spherical coordinates in conjunction with use of the identity, $\partial r^2\delta(r)/\partial r = 0$, that also results in a homogeneous wave equation. Note that for $c_2 = 0$ within Eq. 67 a solution of the Helmholtz equation is found.

Implementation

We now present the process of numerically evaluating Eq. 26 for the spectral density of acoustic pressure ($k = 4$). The spectral representations contain arguments that are presented in Eqs. 41 through 44. Analytical solutions for the vector Green's function (for a quiescent field), $\hat{q}_{g,k}^{\perp n}$, and its complex conjugate, $\hat{q}_{g,k}^{*\perp m}$, were developed in the previous section. We make use of $\hat{p}_g^{\perp,n}$ ($k = 4$) for $\hat{q}_{g,k}^{\perp n}$ and $\hat{p}_g^{*\perp,n}$ for $\hat{q}_{g,k}^{*\perp m}$. The integrand

involving $\boldsymbol{y}$ involves the double summation over m and n and is easily implemented in a computer program. We assume (for convenience) $x >> L$ and that the isotropic turbulence is contained within a period box with lengths L and approximate the volumetric integral involving $d\boldsymbol{y}$ as L^3. The model Eq. 26 is evaluated at each observer position $\boldsymbol{x}$ for each desired unit bandwidth f at $\omega = 2\pi f$. The arguments of κ, κ_1, and κ_2 within the limits of Eqs. 41 through 44 are related to ω as $\kappa_2 - \kappa_1 = 2\pi c_\infty^{-1}$ and centered about $\omega = c_\infty \kappa$.

Results

This section shows predictions using the newly developed theories and compares them with corresponding numerical predictions and measurements from various sources. Most importantly, we compare our source model to results from DNS and compare predicted power spectra of acoustic pressure with those derived from DNS.

Aerodynamics

Figure 2 shows the decay of pressure covariance within an isotropic field with an initial integral Reynolds number of 6328. The x-axis represents retarded time normalized by $\omega_o = 2\pi\mathcal{T}^{-1}$, where $\mathcal{T}$ is the initial integral time scale. Data from the DNS of Debussche et al.,[48] which also was conducted at $\mathcal{R}e_L = 6328$ using a 'multi-level' method on 512^3 grid points, are shown as circles. The model from Lilley[29] is shown as a dash-dot-dot line. Equation 39 is shown as a series of lines labeled ι_c, where ι_c varies from zero through one. Recall that when $\iota_c = 1$, Gaussian statistics of the source are assumed, and the model nearly aligns with the DNS results of Debussche et al.[48] For $\iota_c = 0.80$, nearly perfect agreement is observed between Eq. 39 and the DNS results of Debussche et al.[48] A purely exponentially decaying model, which corresponds to $\iota_c = 0$, shows very little promise relative to the model of Lilley[29] or the numerical result. It is interesting to consider that at relatively large integral times scales (from initial period of decay) that $\iota_c = 0.40$ agrees extremely well with the model of Lilley.[29] A mixed Gaussian-exponential decaying model is best suited to what is observed in DNS simulations. Though the use of $\iota_c = 0.8$ likely yields the most accurate result, it is considerably more difficult to work with mathematically. Because the differences between the Gaussian and mixed Gaussian-exponential model are so small, and the agreement is satisfactory compared to DNS results, we elect to continue our investigation with a purely Gaussian model.

We now examine the decay of the correlation of pressure with time on a wavenumber basis. Figures 3 and 4 show the model decay compared to the DNS results of Yao et al.[34] at two conditions. The conditions correspond to stationary isotropic turbulence at $\mathcal{R}e_\lambda$ of 78.75 and 148.92 with corresponding $\mathcal{L} = 1.597$ m and 1.471 m, and $\lambda = 0.599$ m and 0.341 m, in Figs. 3 and 4, respectively. Simulations of Yao et al.[34] were contained within a domain with sides of length 2π m and contained 128^3 and 256^3 nodes, respectively. On a wavenumber basis the pressure correlation is defined as $\langle p(\kappa,\tau)p(-\kappa,t+\tau)\rangle \langle p(\kappa,\tau)\rangle^{-1} \langle p(\kappa,-\tau)\rangle^{-1}$. At relatively small wavenumbers the model agrees well with the DNS of Yao et al.[34] at both $\mathcal{R}e_\lambda$ of 78.75 and 148.92. At higher wavenumbers, the model decays at a slower rate than the numerical results. The pressure covariance decay within the DNS simulation is Gaussian in nature and is captured by the model. It is well known that the wavenumber goes as $\exp\left[-\alpha\kappa^2\right]$, where α is a positive constant coefficient. This trend is captured explicitly in the model (see Eq. 39) but does not seem to appear in this particular DNS result, at least not for the pressure covariance. Note that the developed two-point cross-correlation model, which the model results here are based upon, is evaluated for all the statistics. The results would greatly be improved if $\boldsymbol{R}$ was modeled for each particular term. Here, we continue with the simplified approach of using a single model to capture the trend of all two-point cross-correlations.

An example comparison of the energy spectrum, E_u, of Eq. 48 and the DNS results of Seror et al.[44] is shown in Fig. 5. The DNS of Seror et al.[44] used 192^3 grid points, had a Taylor Reynolds number, $\mathcal{R}e_\lambda = 82.31$, integral length scale, $\mathcal{L} = 0.98$ m, Taylor length scale, $\lambda = 0.28$ m, and Kolmogorov length scale, $\eta = 0.02$ m. The y-axis represents E_u normalized by the total energy of E_u and the x-axis is the wavenumber, κ. The model is evaluated using the same conditions as Seror et al.[44] A dashed line is added to the figure that represents the $\kappa^{-5/3}$ law of Kolmogorov.[2] In the inertial range, both the DNS and three-dimensional velocity energy spectrum of Kolmogorov (within Eq. 48) are in good agreement. The overall levels between the DNS results of Seror et al.[44] and the model compare well.

We now examine the wavenumber energy spectrum, E_u, on a frequency basis in Fig. 6. The spectrum corresponds to the DNS of Witkowska et al.[43] Turbulence is isotropic and stationary, and the DNS was

performed at conditions corresponding to $\mathcal{R}e_\lambda = 20$ and $u'_{rms}c_\infty^{-1} = 0.01$. The computational domain of Witkowska et al.[43] is 14.3 times larger than $\mathcal{L}$ and contains 128^3 points. As in Fig. 5, the spectrum has been normalized by the total energy within E_u. The x-axis is normalized by $\mathcal{L}$ and u'_{rms}. At characteristic eddy frequencies ($\omega\mathcal{L}u'^{-1}_{rms}$) of unity and above the composite spectrum of Pope[10] agrees very well with the DNS results of Witkowska et al.[43] At lower characteristic eddy frequencies, the model composite spectrum falls off much faster than the DNS results, which is surprising given the very large domain ($14.3\mathcal{L}$) used in the DNS.

We now turn our attention to comparing models of the statistics and wavenumber spectra of decaying isotropic turbulence to DNS results and measurement. Sarkar and Hussaini[42] conducted DNS studies of stationary and decaying isotropic turbulence. The turbulent field was initialized and allowed to evolve into fully developed isotropic turbulence; then production was turned off and the turbulence began to decay. At the beginning of decay ($\tau = 0$) $\mathcal{R}e_\lambda = 50$ and $M_t = 0.05$, which correspond to $L = 0.58$ m, $\lambda = 0.12$ m, and $\eta = 0.03$ m. Decay was simulated for approximately 15 eddy turnover times. Initial $k_o = 0.4404 \times 10^3$ m^{2}s^{-2} and $\epsilon_o = 0.34232 \times 10^8$ m^{2}s^{-3}. The computational domain consisted of 128^3 grid points. Figures 7 and 8 show the decay of k and ϵ from the results of the DNS of Sarkar and Hussaini[42] as lines with squares. Corresponding predictions from the developed model are shown as black lines. The y-axis is normalized by the initial k or ϵ as reported by Sarkar and Hussaini,[42] and the x-axis (time) is normalized by $\epsilon_o\kappa_o^{-1}$. Note initially the DNS results of Sarkar and Hussaini[42] are undergoing a transformation from stationary isotropic turbulence to decaying isotropic turbulence. In the next subsection, we will reexamine these DNS results of Sarkar and Hussaini[42] with respect to decaying sound power.

We have compared our model predictions for k and ϵ with the DNS data of Sarkar and Hussaini[42] in Figs. 7 and 8. A similar set of DNS results were produced by Lesieur et al.,[19] and they examined the decay of k and $\langle TT\rangle/2$. Comparisons between the model predictions and the DNS results of Lesieur et al.[19] are shown in Fig. 9. The model is evaluated at $\mathcal{R}e_t = 50000$, $\mathcal{R}e_\lambda = 577$, and $u'_{rms} = 0.4112$ m^{2}s^{-2}. Length scales are $\mathcal{L} = 1.5$ m, $\lambda = 0.0212$ m, and $\eta = 4.486 \times 10^{-4}$ m. Initial turbulent statistics are $k_0 = 0.25368$ m^{2}s^{-2} and $\epsilon_0 = 0.08518$ m^{2}s^{-3}. The reported Reynolds number of Lesieur et al.[19] is 40000 at $\tau = 0$. The x-axis is the source time, τ, normalized by the large-eddy turn-over time $\mathcal{T}$. The model predicts a slightly lower rate of decay of k and $\langle TT\rangle/2$ relative to the DNS results of Lesieur et al.[19] Both the model and DNS results show an exponential decay of k and $\langle TT\rangle/2$. It is encouraging that the exponential decay is similar to that observed in the DNS results of Sarkar and Hussaini.[42] The decay coefficient of -0.31 within Eq. 60 arguably should be increased slightly for the results to better match DNS simulation, but the coefficient was chosen based on measurement data of isotropic turbulence behind grids.

We now examine the variation of energy spectra within decaying isotropic turbulence. Extensive measurements of E_u, among many other statistical quantities, were made by Stewart and Townsend.[7] These measurements were obtained within grid turbulence, which is a flow that has gone through a grid with periodic spacing M. Immediately downstream of the grid the flow is highly anisotropic and slowly becomes isotropic. Figure 10 shows measurements of E_u normalized by the total energy of E_u of Stewart and Townsend[7] at various non-dimensional distances downstream xM^{-1}, where x is the downstream distance. The flow properties are defined by grid Reynolds number, $\mathcal{R}e_M = Mu_\infty\nu_\infty^{-1} = 5300$, $M = 0.0508$ m, and $u_\infty = 6.2$ ms^{-1}. The x-axis corresponds to wavenumber normalized by the local λ at corresponding xM^{-1}. Results are presented at distances $xM^{-1} = 30$ through 120 downstream from the grid. Stewart and Townsend[7] presented their results in this format to convince the reader of the collapse of the inertial range when normalized by $\kappa\lambda$. Normalized spectra near the grid show a very pronounced lobe. As an example, there is a large lobe at $\kappa\lambda \approx 0.4$ and $xM^{-1} = 30$. Predictions using the developed equations for the decay of k, ϵ, and E_u are shown as various line types without symbols. These predictions do not capture the strong broad lobes at lower wavenumber as the composite spectrum cannot explicitly capture this particular anisotropic effect of grid turbulence. Recall that the developed prediction model is dependent on time, while the experiments included a convection time due to spacing of axial measurement locations. We have attempted to directly compare decay time with convection decay time in these comparisons. Within the inertial range, the measurements of Stewart and Townsend[7] and the predictions of E_u increase slightly then approach an asymptotic value. At low $\kappa\lambda$, there is no collapse possible of either prediction or measurement; however, both decay with increasing $\lambda\kappa$.

The decay of the temperature spectrum, E_T, was investigated numerically by Lesieur et al.,[19] and the conditions of their simulation correspond to the previous discussion on decay of k and $\langle TT\rangle$. Recall the initial conditions are $\mathcal{R}e_t = 5 \times 10^4$, $\mathcal{L} = 1.5$ m, $\lambda = 0.0212$ m, and $\eta = 4.486 \times 10^{-4}$ m. Figure 11 shows E_T at

various times normalized by the large-eddy turn-over time $\mathcal{T}$. Lines with symbols are the results of Lesieur et al.[19] and corresponding line types without symbols are predictions based upon the developed decay model. The simulation encompasses large-eddy turnover times from $\tau\mathcal{T}^{-1} \approx 6$ to 12. As time increases, the peak κ of E_T decreases, the 'energy' of E_T decreases, and the inertial range remains fully developed and decreases with κ. In the wavenumber range between the peak of E_T and large wavelengths, the predicted E_T and numerically simulated E_T are in relatively good agreement. At low wavenumbers, the slope of predicted E_T and simulation are inconsistent, and this could be corrected by modifying the function f_L that operates on E_T.

Aeroacoustics

The power spectrum of acoustic pressure from a differential element of isotropic turbulence is shown in Fig. 12. Comparisons are conducted on a sound pressure level (SPL) per unit $\mathcal{S}t$ basis, where $\mathcal{S}t = fLk^{-1/2}$. The results correspond to turbulence at $\mathcal{R}e_\lambda = 50$ and $M_t = 0.05$. The DNS prediction of Sarkar and Hussaini[42] is shown as squares, where the results were scaled on a volumetric basis for comparison. Power spectra from the DNS were calculated by Sarkar and Hussaini[42] by approximating the Lighthill stress tensor directly from the DNS simulation and subsequently finding the time varying pressure fluctuation at the far-field observer. The DNS was conducted on a grid containing 128^3 points. The prediction from Eq. 26 for $k = 4$ is shown as a solid line. The source spectrum developed by Lilley[29] is superimposed on the results for comparison. The SPL at the peak frequency is in excellent agreement between the prediction and numerical simulation. At low frequencies, the prediction matches numerical simulation and at high frequencies shows a slightly lower rate of decay. The prediction agrees well with the result of Seror et al.[44] and at high frequencies exhibits some divergence.

Figure 13 shows the power spectrum of acoustic pressure from stationary isotropic turbulence. The turbulence contains properties corresponding to $\mathcal{R}e_\lambda = 20$ and $M_t = 0.010$, and the computational domain contains 128^3 grid points. The turbulent field is restricted to a cube with sides that are 14.3 times larger than the integral length scale. Witkowska et al.[43] found the power spectrum using a similar approach as Sarkar and Hussaini[42] at a point $286L$ from the center of the turbulent field. Their calculation is shown as a dashed line. The developed prediction approach of Eq. 26 for $k = 4$ is shown as a solid line. Predicted peak frequencies and maximum power spectra are in close agreement. Note that the DNS simulations are conducted at relatively low $\mathcal{R}e$, and the developed theory assumes high $\mathcal{R}e$.

A final comparison is shown in Figure 14 for the overall sound pressure level per unit $\epsilon_o k_o^{-1}$ within a decaying isotropic field. Here, k_o and ϵ_o are the initial turbulent kinetic energy and dissipation of the DNS of Sarkar and Hussaini.[42] As previously discussed, the properties of the turbulence correspond to $\mathcal{R}e_\lambda = 50$ and $M_t = 0.05$. The DNS result of Sarkar and Hussaini[42] is shown as a line with squares, the theory of Proudman[25] is shown as a dashed line, and the prediction is shown as a solid line. The prediction based on Lilley's[29] theory is not directly applicable because it was mainly developed for the eventual purpose of jet noise prediction, but it would follow the present trends. Note that the DNS result is an ensemble averaged overall SPL from multiple simulations, and it is likely that the small oscillations in the DNS result would diminish with increased averages. The application of the theory of Proudman[25] decays at almost a constant rate, but this is deceiving as ϵ and M_t vary as τ increases. The relative magnitude of the prediction of the present theory varies from two to six overall SPL per unit $\epsilon_o k_o$ dB above the DNS result of Sarkar and Hussaini.[42] The current theory, the theory of Proudman,[25] and the DNS result of Sarkar and Hussaini[42] decay at approximately the same rate over multiple large-eddy turn-over times.

Conclusion

We have presented a new method to predict acoustic radiation from stationary and decaying isotropic turbulence. This is accomplished by decomposing the Navier-Stokes equations into anisotropic and isotropic components and solving for the radiating terms. The anisotropic radiation and corresponding sources are equated to zero as the flow is assumed to be fully isotropic. Two-point cross-correlations of the equivalent source are derived, and a simplified form is proposed. The simplified form of the normalized two-point cross-correlation is validated with measurement and numerical simulation. The predictions can be improved by independently calibrating the coefficients within the simplified two-point cross-correlation for each source term combination, or simply by including a small positive non-zero constant involving the exponential decay

term involving the wavenumber. Scaling of the source is a function of its time and length scale, and most importantly, directly related to wavenumber spectra of each field-variable. Wavenumber spectra are taken from canonical results of the statistical theory of turbulence and represent some of the only exact solutions in the field of fluid dynamics.

Unfortunately, theoretical fluid dynamics is limited and not all the scaling powers of the wavenumber spectra are known, let alone the prefactor constants. This method and the general theory of turbulence can be greatly improved if the exact constants and powers are derived analytically for all wavenumber spectra of the field variables. A simplistic method is developed to predict the decaying turbulent statistics and decaying wavenumber spectra of isotropic turbulence. Comparisons of predictions using this method with measurement and direct numerical simulation results showed only satisfactory agreement, and it is clear that present decay theory is very limited. A solution for the vector Green's function, particularly for acoustic pressure, is presented that closes the model equation. This set of equations can be solved for other types of time-evolving base flows or stationary flows, or include solid bodies for scattering calculations. The model equation is evaluated using the previously developed and validated arguments. Predictions of the acoustic pressure from a stationary isotropic field agree well with results derived from direct numerical simulation and previous theory. Predicted total acoustic power from a decaying field of isotropic turbulence yields results that compare well with theory and the numerical simulation.

Wavenumber spectra theory of structure functions is generally limited to high Reynolds number while direct numerical simulation is limited to low Reynolds number. There are clear differences between the predictions that are dependent on wavenumber spectra and those that are derived by direct numerical simulation. These differences will hopefully be eliminated as results derived by high Reynolds number direct numerical simulation become available in the future. Unfortunately, power coefficients (e.g., density) of the wavenumber spectra of structure functions are unknown for certain field variables. The present theory and the theory of turbulence would be greatly advanced if analytical results can be derived for the composite wavenumber spectra or even just the inertial range. Finally, it is hopeful that the anisotropic portion of this theory can be quantified for certain canonical flow-fields to further validate this new theory.

Acknowledgments

The author is inspired by the life and work of Andrei Nikolaevich Kolmogorov. The photographs of isotropic turbulence in Fig. 1 are courtesy of Hesselink and Sturtevant[6] and used with written permission.

Appendix: Two-Point Cross-Correlations for Isotropic Turbulence

This appendix shows the full form of the two-point space-time cross-correlation using the decomposition of Eq. 6, the definition of the sources in Eqs. 9 through 11, and the definition of $R^{\perp}_{m,n}$ in Eq. 25. The superscript (1) or (2) signifies that the quantity is evaluated at position $\boldsymbol{y}$ or $\boldsymbol{y}+\boldsymbol{\eta}$, respectively. Note that some terms are not explicitly shown (e.g., $m \neq n$ and $n > m$) as they are easily derived by substitution of m for n and i, j, and k for l, m, and n. The continuity-continuity ($m = n = 0$) two-point space-time cross-correlation is

$$\begin{aligned} R^{\perp}_{0,0}\left(\boldsymbol{y},\boldsymbol{\eta},\tau\right) = &\left\langle \frac{\partial\tilde{\overline{\rho}}^{(1)}}{\partial\tau}, \frac{\partial\tilde{\overline{\rho}}^{(2)}}{\partial\tau} \right\rangle + 2\left\langle \frac{\partial\overline{\rho}^{(1)}\tilde{\overline{u}}_j^{(1)} + \tilde{\overline{\rho}}^{(1)}\tilde{\overline{u}}_j^{(1)}}{\partial y_j}, \frac{\partial\tilde{\overline{\rho}}^{(2)}}{\partial\tau} \right\rangle \\ &+ \left\langle \frac{\partial\overline{\rho}^{(1)}\tilde{\overline{u}}_j^{(1)} + \tilde{\overline{\rho}}^{(1)}\tilde{\overline{u}}_j^{(1)}}{\partial y_j}, \frac{\partial\overline{\rho}^{(2)}\tilde{\overline{u}}_m^{(2)} + \tilde{\overline{\rho}}^{(2)}\tilde{\overline{u}}_m^{(2)}}{\partial y_m} \right\rangle. \end{aligned} \tag{68}$$

The continuity-momentum ($m = 0$ and $n = 1$ to 3) two-point space-time cross-correlation is

$$\begin{aligned} R^{\perp}_{0,l}\left(\boldsymbol{y},\boldsymbol{\eta},\tau\right) = &\left\langle \frac{\partial\tilde{\overline{\rho}}^{(1)}}{\partial\tau}, \frac{\partial}{\partial\tau}\left[\overline{\rho}^{(2)}\tilde{\overline{u}}_l^{(2)} + \tilde{\overline{\rho}}^{(2)}\tilde{\overline{u}}_l^{(2)}\right] \right\rangle + \left\langle \frac{\partial\tilde{\overline{\rho}}^{(1)}}{\partial\tau}, \frac{\partial}{\partial y_m}\left[(\overline{\rho}^{(2)} + \tilde{\overline{\rho}}^{(2)})\tilde{\overline{u}}_l^{(2)}\tilde{\overline{u}}_m^{(2)}\right] \right\rangle \\ &+ \left\langle -\frac{\partial\tilde{\overline{\rho}}^{(1)}}{\partial\tau}, \frac{\partial\overline{\mu}}{\partial y_m}\left[\frac{\partial\tilde{\overline{u}}_l^{(2)}}{\partial y_m} + \frac{\partial\tilde{\overline{u}}_m^{(2)}}{\partial y_l}\right] \right\rangle + \left\langle \frac{\partial\tilde{\overline{\rho}}^{(1)}}{\partial\tau}, \frac{2}{3}\frac{\partial}{\partial y_m}\left\{\overline{\mu}\frac{\partial}{\partial y_n}\tilde{\overline{u}}_n^{(2)}\right\} \right\rangle + \left\langle \frac{\partial\tilde{\overline{\rho}}^{(1)}}{\partial\tau}, \frac{\partial\tilde{\overline{p}}^{(2)}}{\partial y_m}\delta_{lm} \right\rangle \\ &+ \left\langle \frac{\partial(\overline{\rho}^{(1)} + \tilde{\overline{\rho}}^{(1)})\tilde{\overline{u}}_j^{(1)}}{\partial y_j}, \frac{\partial}{\partial\tau}\left[\overline{\rho}^{(2)}\tilde{\overline{u}}_l^{(2)} + \tilde{\overline{\rho}}^{(2)}\tilde{\overline{u}}_l^{(2)}\right] \right\rangle + \left\langle \frac{\partial(\overline{\rho}^{(1)} + \tilde{\overline{\rho}}^{(1)})\tilde{\overline{u}}_j^{(1)}}{\partial y_j}, \frac{\partial}{\partial y_m}\left[(\overline{\rho}^{(2)} + \tilde{\overline{\rho}}^{(2)})\tilde{\overline{u}}_l^{(2)}\tilde{\overline{u}}_m^{(2)}\right] \right\rangle \\ &+ \left\langle -\frac{\partial(\overline{\rho}^{(1)} + \tilde{\overline{\rho}}^{(1)})\tilde{\overline{u}}_j^{(1)}}{\partial y_j}, \frac{\partial\overline{\mu}}{\partial y_m}\left[\frac{\partial\tilde{\overline{u}}_l^{(2)}}{\partial y_m} + \frac{\partial\tilde{\overline{u}}_m^{(2)}}{\partial y_l}\right] \right\rangle + \left\langle \frac{2}{3}\frac{\partial(\overline{\rho}^{(1)} + \tilde{\overline{\rho}}^{(1)})\tilde{\overline{u}}_j^{(1)}}{\partial y_j}, \frac{\partial}{\partial y_m}\left\{\overline{\mu}\frac{\partial}{\partial y_n}\tilde{\overline{u}}_n^{(2)}\right\} \right\rangle \\ &+ \left\langle \frac{\partial(\overline{\rho}^{(1)} + \tilde{\overline{\rho}}^{(1)})\tilde{\overline{u}}_j^{(1)}}{\partial y_j}, \frac{\partial\tilde{\overline{p}}^{(2)}}{\partial y_m}\delta_{lm} \right\rangle. \end{aligned} \tag{69}$$

The continuity-energy ($m = 0$ and $n = 4$) two-point space-time cross-correlation is

$$\begin{aligned} R^{\perp}_{0,4}\left(\boldsymbol{y},\boldsymbol{\eta},\tau\right) = &\left\langle \frac{\partial\tilde{\overline{\rho}}^{(1)}}{\partial\tau}, \frac{\partial\tilde{\overline{p}}^{(2)}}{\partial\tau} \right\rangle + \left\langle \frac{\gamma-1}{2}\frac{\partial\tilde{\overline{\rho}}^{(1)}}{\partial\tau}, \frac{\partial\tilde{\overline{\rho}}^{(2)}\tilde{\overline{u}}_n^{2,(2)}}{\partial\tau} \right\rangle + \left\langle \frac{\partial\tilde{\overline{\rho}}^{(1)}}{\partial\tau}, \gamma\frac{\partial\tilde{\overline{u}}_m^{(2)}(\overline{p}^{(2)} + \tilde{\overline{p}}^{(2)})}{\partial y_m} \right\rangle \\ &+ \left\langle \frac{\gamma-1}{2}\frac{\partial\tilde{\overline{\rho}}^{(1)}}{\partial\tau}, \frac{\partial(\overline{\rho}^{(2)} + \tilde{\overline{\rho}}^{(2)})\tilde{\overline{u}}_m^{(2)}\tilde{\overline{u}}_n^{(2)}\tilde{\overline{u}}_n^{(2)}}{\partial y_m} \right\rangle + \left\langle -(\gamma-1)\frac{\partial\tilde{\overline{\rho}}^{(1)}}{\partial\tau}, \frac{\overline{c}_p\overline{\mu}}{\overline{Pr}}\frac{\partial^2}{\partial y_m\partial y_m}\left[\overline{T}^{(2)} + \tilde{\overline{T}}^{(2)}\right] \right\rangle \\ &+ \left\langle -(\gamma-1)\frac{\partial\tilde{\overline{\rho}}^{(1)}}{\partial\tau}, \overline{\mu}\frac{\partial}{\partial y_m}\left[\tilde{\overline{u}}_l^{(2)}\left(\frac{\partial\tilde{\overline{u}}_l^{(2)}}{\partial y_m} + \frac{\partial\tilde{\overline{u}}_m^{(2)}}{\partial y_l}\right)\right] \right\rangle + \left\langle \frac{2}{3}\frac{\partial\tilde{\overline{\rho}}^{(1)}}{\partial\tau}, \delta_{lm}\overline{\mu}\frac{\partial}{\partial y_m}\left[\tilde{\overline{u}}_l^{(2)}\frac{\partial\tilde{\overline{u}}_n^{(2)}}{\partial y_n}\right] \right\rangle \\ &+ \left\langle \frac{\partial\overline{\rho}^{(1)}\tilde{\overline{u}}_j^{(1)} + \tilde{\overline{\rho}}^{(1)}\tilde{\overline{u}}_j^{(1)}}{\partial y_j}, \frac{\partial\tilde{\overline{p}}^{(2)}}{\partial\tau} \right\rangle + \left\langle \frac{\gamma-1}{2}\frac{\partial\overline{\rho}^{(1)}\tilde{\overline{u}}_j^{(1)} + \tilde{\overline{\rho}}^{(1)}\tilde{\overline{u}}_j^{(1)}}{\partial y_j}, \frac{\partial\tilde{\overline{\rho}}^{(2)}\tilde{\overline{u}}_k^{2,(2)}}{\partial\tau} \right\rangle + \left\langle \frac{\partial\overline{\rho}^{(1)}\tilde{\overline{u}}_j^{(1)} + \tilde{\overline{\rho}}^{(1)}\tilde{\overline{u}}_j^{(1)}}{\partial y_j}, \gamma\frac{\partial\tilde{\overline{u}}_m^{(2)}(\overline{p}^{(2)} + \tilde{\overline{p}}^{(2)})}{\partial y_m} \right\rangle \\ &+ \left\langle \frac{\gamma-1}{2}\frac{\partial\overline{\rho}^{(1)}\tilde{\overline{u}}_j^{(1)} + \tilde{\overline{\rho}}^{(1)}\tilde{\overline{u}}_j^{(1)}}{\partial y_j}, \frac{\partial(\overline{\rho}^{(2)} + \tilde{\overline{\rho}}^{(2)})\tilde{\overline{u}}_m^{(2)}\tilde{\overline{u}}_n^{(2)}\tilde{\overline{u}}_n^{(2)}}{\partial y_m} \right\rangle + \left\langle -(\gamma-1)\frac{\partial\overline{\rho}^{(1)}\tilde{\overline{u}}_j^{(1)} + \tilde{\overline{\rho}}^{(1)}\tilde{\overline{u}}_j^{(1)}}{\partial y_j}, \frac{\overline{c}_p\overline{\mu}}{\overline{Pr}}\frac{\partial^2}{\partial y_m\partial y_m}\left[\overline{T}^{(2)} + \tilde{\overline{T}}^{(2)}\right] \right\rangle \\ &+ \left\langle -(\gamma-1)\frac{\partial\overline{\rho}^{(1)}\tilde{\overline{u}}_j^{(1)} + \tilde{\overline{\rho}}^{(1)}\tilde{\overline{u}}_j^{(1)}}{\partial y_j}, \overline{\mu}\frac{\partial}{\partial y_m}\left[\tilde{\overline{u}}_l^{(2)}\left(\frac{\partial\tilde{\overline{u}}_l^{(2)}}{\partial y_m} + \frac{\partial\tilde{\overline{u}}_m^{(2)}}{\partial y_l}\right)\right] \right\rangle + \left\langle \frac{2}{3}\frac{\partial\overline{\rho}^{(1)}\tilde{\overline{u}}_j^{(1)} + \tilde{\overline{\rho}}^{(1)}\tilde{\overline{u}}_j^{(1)}}{\partial y_j}, \delta_{lm}\overline{\mu}\frac{\partial}{\partial y_m}\left[\tilde{\overline{u}}_l^{(2)}\frac{\partial\tilde{\overline{u}}_n^{(2)}}{\partial y_n}\right] \right\rangle. \end{aligned} \tag{70}$$

The momentum-momentum ($m = 1$ to 3 and $n = 1$ to 3) two-point space-time cross-correlation is

$$
\begin{aligned}
R^{\perp}_{i,l}(\boldsymbol{y},\boldsymbol{\eta},\tau) = {} & \left\langle \frac{\partial}{\partial\tau}\left[(\overline{\rho}^{(1)}+\tilde{\rho}^{(1)})\tilde{u}_i^{(1)}\right], \frac{\partial}{\partial\tau}\left[(\overline{\rho}^{(2)}+\tilde{\rho}^{(2)})\tilde{u}_l^{(2)}\right]\right\rangle + \left\langle \frac{\partial}{\partial\tau}\left[(\overline{\rho}^{(1)}+\tilde{\rho}^{(1)})\tilde{u}_i^{(1)}\right], \frac{\partial}{\partial y_m}\left[(\overline{\rho}^{(2)}+\tilde{\rho}^{(2)})\tilde{u}_l^{(2)}\tilde{u}_m^{(2)}\right]\right\rangle \\
& + \left\langle \frac{\partial}{\partial\tau}\left[(\overline{\rho}^{(1)}+\tilde{\rho}^{(1)})\tilde{u}_i^{(1)}\right], -\overline{\mu}\frac{\partial}{\partial y_m}\left[\frac{\partial\tilde{u}_l^{(2)}}{\partial y_m}+\frac{\partial\tilde{u}_m^{(2)}}{\partial y_l}\right]\right\rangle + \left\langle \frac{\partial}{\partial\tau}\left[(\overline{\rho}^{(1)}+\tilde{\rho}^{(1)})\tilde{u}_i^{(1)}\right], \overline{\mu}\frac{2}{3}\frac{\partial}{\partial y_m}\left\{\frac{\partial}{\partial y_n}\tilde{u}_n^{(2)}\right\}\right\rangle \\
& + \left\langle \frac{\partial}{\partial\tau}\left[(\overline{\rho}^{(1)}+\tilde{\rho}^{(1)})\tilde{u}_i^{(1)}\right], \frac{\partial\tilde{\rho}^{(2)}}{\partial y_m}\delta_{lm}\right\rangle + \left\langle \frac{\partial}{\partial y_j}\left[(\overline{\rho}^{(1)}+\tilde{\rho}^{(1)})\tilde{u}_i^{(1)}\tilde{u}_j^{(1)}\right], \frac{\partial}{\partial\tau}\left[(\overline{\rho}^{(2)}+\tilde{\rho}^{(2)})\tilde{u}_l^{(2)}\right]\right\rangle \\
& + \left\langle \frac{\partial}{\partial y_j}\left[(\overline{\rho}^{(1)}+\tilde{\rho}^{(1)})\tilde{u}_i^{(1)}\tilde{u}_j^{(1)}\right], \frac{\partial}{\partial y_m}\left[(\overline{\rho}^{(2)}+\tilde{\rho}^{(2)})\tilde{u}_l^{(2)}\tilde{u}_m^{(2)}\right]\right\rangle + \left\langle \frac{\partial}{\partial y_j}\left[(\overline{\rho}^{(1)}+\tilde{\rho}^{(1)})\tilde{u}_i^{(1)}\tilde{u}_j^{(1)}\right], -\overline{\mu}\frac{\partial}{\partial y_m}\left[\frac{\partial\tilde{u}_l^{(2)}}{\partial y_m}+\frac{\partial\tilde{u}_m^{(2)}}{\partial y_l}\right]\right\rangle \\
& + \left\langle \frac{\partial}{\partial y_j}\left[(\overline{\rho}^{(1)}+\tilde{\rho}^{(1)})\tilde{u}_i^{(1)}\tilde{u}_j^{(1)}\right], \overline{\mu}\frac{2}{3}\frac{\partial}{\partial y_m}\left\{\frac{\partial}{\partial y_n}\tilde{u}_n^{(2)}\right\}\right\rangle + \left\langle \frac{\partial}{\partial y_j}\left[(\overline{\rho}^{(1)}+\tilde{\rho}^{(1)})\tilde{u}_i^{(1)}\tilde{u}_j^{(1)}\right], \frac{\partial\tilde{\rho}^{(2)}}{\partial y_m}\delta_{lm}\right\rangle \\
& + \left\langle -\overline{\mu}\frac{\partial}{\partial y_j}\left[\frac{\partial\tilde{u}_i^{(1)}}{\partial y_j}+\frac{\partial\tilde{u}_j^{(1)}}{\partial y_i}\right], \frac{\partial}{\partial\tau}\left[(\overline{\rho}^{(2)}+\tilde{\rho}^{(2)})\tilde{u}_l^{(2)}\right]\right\rangle + \left\langle -\overline{\mu}\frac{\partial}{\partial y_j}\left[\frac{\partial\tilde{u}_i^{(1)}}{\partial y_j}+\frac{\partial\tilde{u}_j^{(1)}}{\partial y_i}\right], \frac{\partial}{\partial y_m}\left[(\overline{\rho}^{(2)}+\tilde{\rho}^{(2)})\tilde{u}_l^{(2)}\tilde{u}_m^{(2)}\right]\right\rangle \\
& + \left\langle -\overline{\mu}\frac{\partial}{\partial y_j}\left[\frac{\partial\tilde{u}_i^{(1)}}{\partial y_j}+\frac{\partial\tilde{u}_j^{(1)}}{\partial y_i}\right], -\overline{\mu}\frac{\partial}{\partial y_m}\left[\frac{\partial\tilde{u}_l^{(2)}}{\partial y_m}+\frac{\partial\tilde{u}_m^{(2)}}{\partial y_l}\right]\right\rangle + \left\langle -\overline{\mu}\frac{\partial}{\partial y_j}\left[\frac{\partial\tilde{u}_i^{(1)}}{\partial y_j}+\frac{\partial\tilde{u}_j^{(1)}}{\partial y_i}\right], \overline{\mu}\frac{2}{3}\frac{\partial}{\partial y_m}\left\{\frac{\partial}{\partial y_n}\tilde{u}_n^{(2)}\right\}\right\rangle \\
& + \left\langle -\overline{\mu}\frac{\partial}{\partial y_j}\left[\frac{\partial\tilde{u}_i^{(1)}}{\partial y_j}+\frac{\partial\tilde{u}_j^{(1)}}{\partial y_i}\right], \frac{\partial\tilde{\rho}^{(2)}}{\partial y_m}\delta_{lm}\right\rangle + \left\langle \frac{2\overline{\mu}}{3}\frac{\partial}{\partial y_j}\left\{\frac{\partial}{\partial y_k}\tilde{u}_k^{(1)}\right\}, \frac{\partial}{\partial\tau}\left[(\overline{\rho}^{(2)}+\tilde{\rho}^{(2)})\tilde{u}_l^{(2)}\right]\right\rangle \\
& + \left\langle \frac{2\overline{\mu}}{3}\frac{\partial}{\partial y_j}\left\{\frac{\partial}{\partial y_k}\tilde{u}_k^{(1)}\right\}, \frac{\partial}{\partial y_m}\left[(\overline{\rho}^{(2)}+\tilde{\rho}^{(2)})\tilde{u}_l^{(2)}\tilde{u}_m^{(2)}\right]\right\rangle + \left\langle \frac{2\overline{\mu}}{3}\frac{\partial}{\partial y_j}\left\{\frac{\partial}{\partial y_k}\tilde{u}_k^{(1)}\right\}, -\overline{\mu}\frac{\partial}{\partial y_m}\left[\frac{\partial\tilde{u}_l^{(2)}}{\partial y_m}+\frac{\partial\tilde{u}_m^{(2)}}{\partial y_l}\right]\right\rangle \\
& + \left\langle \frac{2\overline{\mu}}{3}\frac{\partial}{\partial y_j}\left\{\frac{\partial}{\partial y_k}\tilde{u}_k^{(1)}\right\}, \overline{\mu}\frac{2}{3}\frac{\partial}{\partial y_m}\left\{\frac{\partial}{\partial y_n}\tilde{u}_n^{(2)}\right\}\right\rangle + \left\langle \frac{2\overline{\mu}}{3}\frac{\partial}{\partial y_j}\left\{\frac{\partial}{\partial y_k}\tilde{u}_k^{(1)}\right\}, \frac{\partial\tilde{\rho}^{(2)}}{\partial y_m}\delta_{lm}\right\rangle + \left\langle \frac{\partial\tilde{\rho}^{(1)}}{\partial y_j}\delta_{ij}, \frac{\partial}{\partial\tau}\left[(\overline{\rho}^{(2)}+\tilde{\rho}^{(2)})\tilde{u}_l^{(2)}\right]\right\rangle \\
& + \left\langle \frac{\partial\tilde{\rho}^{(1)}}{\partial y_j}\delta_{ij}, \frac{\partial}{\partial y_m}\left[(\overline{\rho}^{(2)}+\tilde{\rho}^{(2)})\tilde{u}_l^{(2)}\tilde{u}_m^{(2)}\right]\right\rangle + \left\langle \frac{\partial\tilde{\rho}^{(1)}}{\partial y_j}\delta_{ij}, -\overline{\mu}\frac{\partial}{\partial y_m}\left[\frac{\partial\tilde{u}_l^{(2)}}{\partial y_m}+\frac{\partial\tilde{u}_m^{(2)}}{\partial y_l}\right]\right\rangle \\
& + \left\langle \frac{\partial\tilde{\rho}^{(1)}}{\partial y_j}\delta_{ij}, \overline{\mu}\frac{2}{3}\frac{\partial}{\partial y_m}\left\{\frac{\partial}{\partial y_n}\tilde{u}_n^{(2)}\right\}\right\rangle + \left\langle \frac{\partial\tilde{\rho}^{(1)}}{\partial y_j}\delta_{ij}, \frac{\partial\tilde{\rho}^{(2)}}{\partial y_m}\delta_{lm}\right\rangle.
\end{aligned}
\tag{71}
$$

The momentum-energy ($m = 1$ to 3 and $n = 4$) two-point space-time cross-correlation is

$$
\begin{aligned}
R^{\perp}_{i,4}(\boldsymbol{y},\boldsymbol{\eta},\tau) = {} & \left\langle \frac{\partial}{\partial\tau}\left[(\overline{\rho}^{(1)}+\tilde{\rho}^{(1)})\tilde{u}_i^{(1)}\right], \frac{\partial\tilde{p}^{(2)}}{\partial\tau}\right\rangle + \left\langle \frac{\partial}{\partial\tau}\left[(\overline{\rho}^{(1)}+\tilde{\rho}^{(1)})\tilde{u}_i^{(1)}\right], \frac{\gamma-1}{2}\frac{\partial(\overline{p}^{(2)}+\tilde{p}^{(2)})\tilde{u}_n^{2,(2)}}{\partial\tau}\right\rangle \\
& + \left\langle \frac{\partial}{\partial\tau}\left[(\overline{\rho}^{(1)}+\tilde{\rho}^{(1)})\tilde{u}_i^{(1)}\right], \gamma\frac{\partial\tilde{u}_m^{(2)}(\overline{p}^{(2)}+\tilde{p}^{(2)})}{\partial y_m}\right\rangle + \left\langle \frac{\partial}{\partial\tau}\left[(\overline{\rho}^{(1)}+\tilde{\rho}^{(1)})\tilde{u}_i^{(1)}\right], \frac{\gamma-1}{2}\frac{\partial(\overline{p}^{(2)}+\tilde{p}^{(2)})\tilde{u}_m^{(2)}\tilde{u}_n^{(2)}\tilde{u}_n^{(2)}}{\partial y_m}\right\rangle \\
& + \left\langle \frac{\partial}{\partial\tau}\left[(\overline{\rho}^{(1)}+\tilde{\rho}^{(1)})\tilde{u}_i^{(1)}\right], -(\gamma-1)\frac{\overline{c}_p\overline{\mu}}{\overline{Pr}}\frac{\partial}{\partial y_m}\left(\frac{\partial}{\partial y_m}\left[\tilde{T}^{(2)}\right]\right)\right\rangle + \left\langle \frac{\partial}{\partial\tau}\left[(\overline{\rho}^{(1)}+\tilde{\rho}^{(1)})\tilde{u}_i^{(1)}\right], -\overline{\mu}(\gamma-1)\frac{\partial}{\partial y_m}\left[\tilde{u}_l^{(2)}\left(\frac{\partial\tilde{u}_l^{(2)}}{\partial y_m}+\frac{\partial\tilde{u}_m^{(2)}}{\partial y_l}\right)\right]\right\rangle \\
& + \left\langle \frac{\partial}{\partial\tau}\left[(\overline{\rho}^{(1)}+\tilde{\rho}^{(1)})\tilde{u}_i^{(1)}\right], \frac{2\overline{\mu}}{3}\delta_{lm}\frac{\partial}{\partial y_m}\left[\tilde{u}_l^{(2)}\frac{\partial\tilde{u}_n^{(2)}}{\partial y_n}\right]\right\rangle + \left\langle \frac{\partial}{\partial y_j}\left[(\overline{\rho}^{(1)}+\tilde{\rho}^{(1)})\tilde{u}_i^{(1)}\tilde{u}_j^{(1)}\right], \frac{\partial\tilde{p}^{(2)}}{\partial\tau}\right\rangle \\
& + \left\langle \frac{\partial}{\partial y_j}\left[(\overline{\rho}^{(1)}+\tilde{\rho}^{(1)})\tilde{u}_i^{(1)}\tilde{u}_j^{(1)}\right], \frac{\gamma-1}{2}\frac{\partial(\overline{p}^{(2)}+\tilde{p}^{(2)})\tilde{u}_n^{2,(2)}}{\partial\tau}\right\rangle + \left\langle \frac{\partial}{\partial y_j}\left[(\overline{\rho}^{(1)}+\tilde{\rho}^{(1)})\tilde{u}_i^{(1)}\tilde{u}_j^{(1)}\right], \gamma\frac{\partial\tilde{u}_m^{(2)}(\overline{p}^{(2)}+\tilde{p}^{(2)})}{\partial y_m}\right\rangle \\
& + \left\langle \frac{\partial}{\partial y_j}\left[(\overline{\rho}^{(1)}+\tilde{\rho}^{(1)})\tilde{u}_i^{(1)}\tilde{u}_j^{(1)}\right], \frac{\gamma-1}{2}\frac{\partial(\overline{p}^{(2)}+\tilde{p}^{(2)})\tilde{u}_m^{(2)}\tilde{u}_n^{(2)}\tilde{u}_n^{(2)}}{\partial y_m}\right\rangle + \left\langle \frac{\partial}{\partial y_j}\left[(\overline{\rho}^{(1)}+\tilde{\rho}^{(1)})\tilde{u}_i^{(1)}\tilde{u}_j^{(1)}\right], -(\gamma-1)\frac{\overline{c}_p\overline{\mu}}{\overline{Pr}}\frac{\partial}{\partial y_m}\left(\frac{\partial}{\partial y_m}\left[\tilde{T}^{(2)}\right]\right)\right\rangle \\
& + \left\langle \frac{\partial}{\partial y_j}\left[(\overline{\rho}^{(1)}+\tilde{\rho}^{(1)})\tilde{u}_i^{(1)}\tilde{u}_j^{(1)}\right], -\overline{\mu}(\gamma-1)\frac{\partial}{\partial y_m}\left[\tilde{u}_l^{(2)}\left(\frac{\partial\tilde{u}_l^{(2)}}{\partial y_m}+\frac{\partial\tilde{u}_m^{(2)}}{\partial y_l}\right)\right]\right\rangle + \left\langle \frac{\partial}{\partial y_j}\left[(\overline{\rho}^{(1)}+\tilde{\rho}^{(1)})\tilde{u}_i^{(1)}\tilde{u}_j^{(1)}\right], \frac{2\overline{\mu}}{3}\delta_{lm}\frac{\partial}{\partial y_m}\left[\tilde{u}_l^{(2)}\frac{\partial\tilde{u}_n^{(2)}}{\partial y_n}\right]\right\rangle \\
& + \left\langle -\overline{\mu}\frac{\partial}{\partial y_j}\left[\frac{\partial\tilde{u}_i^{(1)}}{\partial y_j}+\frac{\partial\tilde{u}_j^{(1)}}{\partial y_i}\right], \frac{\partial\tilde{p}^{(2)}}{\partial\tau}\right\rangle + \left\langle -\overline{\mu}\frac{\partial}{\partial y_j}\left[\frac{\partial\tilde{u}_i^{(1)}}{\partial y_j}+\frac{\partial\tilde{u}_j^{(1)}}{\partial y_i}\right], \frac{\gamma-1}{2}\frac{\partial(\overline{p}^{(2)}+\tilde{p}^{(2)})\tilde{u}_n^{2,(2)}}{\partial\tau}\right\rangle \\
& + \left\langle -\overline{\mu}\frac{\partial}{\partial y_j}\left[\frac{\partial\tilde{u}_i^{(1)}}{\partial y_j}+\frac{\partial\tilde{u}_j^{(1)}}{\partial y_i}\right], \gamma\frac{\partial\tilde{u}_m^{(2)}(\overline{p}^{(2)}+\tilde{p}^{(2)})}{\partial y_m}\right\rangle + \left\langle -\overline{\mu}\frac{\partial}{\partial y_j}\left[\frac{\partial\tilde{u}_i^{(1)}}{\partial y_j}+\frac{\partial\tilde{u}_j^{(1)}}{\partial y_i}\right], \frac{\gamma-1}{2}\frac{\partial(\overline{p}^{(2)}+\tilde{p}^{(2)})\tilde{u}_m^{(2)}\tilde{u}_n^{(2)}\tilde{u}_n^{(2)}}{\partial y_m}\right\rangle \\
& + \left\langle -\overline{\mu}\frac{\partial}{\partial y_j}\left[\frac{\partial\tilde{u}_i^{(1)}}{\partial y_j}+\frac{\partial\tilde{u}_j^{(1)}}{\partial y_i}\right], -(\gamma-1)\frac{\overline{c}_p\overline{\mu}}{\overline{Pr}}\frac{\partial}{\partial y_m}\left(\frac{\partial}{\partial y_m}\left[\tilde{T}^{(2)}\right]\right)\right\rangle + \left\langle -\overline{\mu}\frac{\partial}{\partial y_j}\left[\frac{\partial\tilde{u}_i^{(1)}}{\partial y_j}+\frac{\partial\tilde{u}_j^{(1)}}{\partial y_i}\right], -\overline{\mu}(\gamma-1)\frac{\partial}{\partial y_m}\left[\tilde{u}_l^{(2)}\left(\frac{\partial\tilde{u}_l^{(2)}}{\partial y_m}+\frac{\partial\tilde{u}_m^{(2)}}{\partial y_l}\right)\right]\right\rangle \\
& + \left\langle -\overline{\mu}\frac{\partial}{\partial y_j}\left[\frac{\partial\tilde{u}_i^{(1)}}{\partial y_j}+\frac{\partial\tilde{u}_j^{(1)}}{\partial y_i}\right], \frac{2\overline{\mu}}{3}\delta_{lm}\frac{\partial}{\partial y_m}\left[\tilde{u}_l^{(2)}\frac{\partial\tilde{u}_n^{(2)}}{\partial y_n}\right]\right\rangle + \left\langle \frac{2\overline{\mu}}{3}\frac{\partial}{\partial y_j}\left\{\frac{\partial}{\partial y_k}\tilde{u}_k^{(1)}\right\}, \frac{\partial\tilde{p}^{(2)}}{\partial\tau}\right\rangle \\
& + \left\langle \frac{2\overline{\mu}}{3}\frac{\partial}{\partial y_j}\left\{\frac{\partial}{\partial y_k}\tilde{u}_k^{(1)}\right\}, \frac{\gamma-1}{2}\frac{\partial(\overline{p}^{(2)}+\tilde{p}^{(2)})\tilde{u}_n^{2,(2)}}{\partial\tau}\right\rangle + \left\langle \frac{2\overline{\mu}}{3}\frac{\partial}{\partial y_j}\left\{\frac{\partial}{\partial y_k}\tilde{u}_k^{(1)}\right\}, \gamma\frac{\partial\tilde{u}_m^{(2)}(\overline{p}^{(2)}+\tilde{p}^{(2)})}{\partial y_m}\right\rangle \\
& + \left\langle \frac{2\overline{\mu}}{3}\frac{\partial}{\partial y_j}\left\{\frac{\partial}{\partial y_k}\tilde{u}_k^{(1)}\right\}, \frac{\gamma-1}{2}\frac{\partial(\overline{p}^{(2)}+\tilde{p}^{(2)})\tilde{u}_m^{(2)}\tilde{u}_n^{(2)}\tilde{u}_n^{(2)}}{\partial y_m}\right\rangle + \left\langle \frac{2\overline{\mu}}{3}\frac{\partial}{\partial y_j}\left\{\frac{\partial}{\partial y_k}\tilde{u}_k^{(1)}\right\}, -(\gamma-1)\frac{\overline{c}_p\overline{\mu}}{\overline{Pr}}\frac{\partial}{\partial y_m}\left(\frac{\partial}{\partial y_m}\left[\tilde{T}^{(2)}\right]\right)\right\rangle \\
& + \left\langle \frac{2\overline{\mu}}{3}\frac{\partial}{\partial y_j}\left\{\frac{\partial}{\partial y_k}\tilde{u}_k^{(1)}\right\}, -\overline{\mu}(\gamma-1)\frac{\partial}{\partial y_m}\left[\tilde{u}_l^{(2)}\left(\frac{\partial\tilde{u}_l^{(2)}}{\partial y_m}+\frac{\partial\tilde{u}_m^{(2)}}{\partial y_l}\right)\right]\right\rangle + \left\langle \frac{2\overline{\mu}}{3}\frac{\partial}{\partial y_j}\left\{\frac{\partial}{\partial y_k}\tilde{u}_k^{(1)}\right\}, \frac{2\overline{\mu}}{3}\delta_{lm}\frac{\partial}{\partial y_m}\left[\tilde{u}_l^{(2)}\frac{\partial\tilde{u}_n^{(2)}}{\partial y_n}\right]\right\rangle \\
& + \left\langle \frac{\partial\tilde{p}^{(1)}}{\partial y_j}\delta_{ij}, \frac{\partial\tilde{p}^{(2)}}{\partial\tau}\right\rangle + \left\langle \frac{\partial\tilde{p}^{(1)}}{\partial y_j}\delta_{ij}, \frac{\gamma-1}{2}\frac{\partial(\overline{p}^{(2)}+\tilde{p}^{(2)})\tilde{u}_n^{2,(2)}}{\partial\tau}\right\rangle \\
& + \left\langle \frac{\partial\tilde{p}^{(1)}}{\partial y_j}\delta_{ij}, \gamma\frac{\partial\tilde{u}_m^{(2)}(\overline{p}^{(2)}+\tilde{p}^{(2)})}{\partial y_m}\right\rangle + \left\langle \frac{\partial\tilde{p}^{(1)}}{\partial y_j}\delta_{ij}, \frac{\gamma-1}{2}\frac{\partial(\overline{p}^{(2)}+\tilde{p}^{(2)})\tilde{u}_m^{(2)}\tilde{u}_n^{(2)}\tilde{u}_n^{(2)}}{\partial y_m}\right\rangle \\
& + \left\langle \frac{\partial\tilde{p}^{(1)}}{\partial y_j}\delta_{ij}, -(\gamma-1)\frac{\overline{c}_p\overline{\mu}}{\overline{Pr}}\frac{\partial}{\partial y_m}\left(\frac{\partial}{\partial y_m}\left[\tilde{T}^{(2)}\right]\right)\right\rangle + \left\langle \frac{\partial\tilde{p}^{(1)}}{\partial y_j}\delta_{ij}, -\overline{\mu}(\gamma-1)\frac{\partial}{\partial y_m}\left[\tilde{u}_l^{(2)}\left(\frac{\partial\tilde{u}_l^{(2)}}{\partial y_m}+\frac{\partial\tilde{u}_m^{(2)}}{\partial y_l}\right)\right]\right\rangle \\
& + \left\langle \frac{\partial\tilde{p}^{(1)}}{\partial y_j}\delta_{ij}, \frac{2\overline{\mu}}{3}\delta_{lm}\frac{\partial}{\partial y_m}\left[\tilde{u}_l^{(2)}\frac{\partial\tilde{u}_n^{(2)}}{\partial y_n}\right]\right\rangle.
\end{aligned}
\tag{72}
$$

The energy-energy ($m = 4$ and $n = 4$) two-point space-time cross-correlation is

$$
\begin{aligned}
R^{\perp}_{4,4}(\boldsymbol{y},\boldsymbol{\eta},\tau) = {} & \left\langle \frac{\partial\tilde{\tilde{p}}^{(1)}}{\partial\tau}, \frac{\partial\tilde{\tilde{p}}^{(2)}}{\partial\tau} \right\rangle + \left\langle \frac{\partial\tilde{\tilde{p}}^{(1)}}{\partial\tau}, \frac{\gamma-1}{2}\frac{\partial(\overline{p}^{(2)}+\tilde{\tilde{p}}^{(2)})\tilde{\tilde{u}}_n^{2,(2)}}{\partial\tau} \right\rangle + \left\langle \frac{\partial\tilde{\tilde{p}}^{(1)}}{\partial\tau}, \gamma\frac{\partial\tilde{\tilde{u}}_m^{(2)}(\overline{p}^{(2)}+\tilde{\tilde{p}}^{(2)})}{\partial y_m} \right\rangle + \left\langle \frac{\partial\tilde{\tilde{p}}^{(1)}}{\partial\tau}, \frac{\gamma-1}{2}\frac{\partial(\overline{p}^{(2)}+\tilde{\tilde{p}}^{(2)})\tilde{\tilde{u}}_m^{(2)}\tilde{\tilde{u}}_n^{(2)}\tilde{\tilde{u}}_n^{(2)}}{\partial y_m} \right\rangle \\
& + \left\langle \frac{\partial\tilde{\tilde{p}}^{(1)}}{\partial\tau}, -(\gamma-1)\frac{\overline{c}_p\overline{\mu}}{\overline{\mathcal{P}r}}\frac{\partial}{\partial y_m}\left(\frac{\partial\tilde{\tilde{T}}^{(2)}}{\partial y_m}\right) \right\rangle + \left\langle \frac{\partial\tilde{\tilde{p}}^{(1)}}{\partial\tau}, -(\gamma-1)\overline{\mu}\frac{\partial}{\partial y_m}\left[\tilde{\tilde{u}}_l^{(2)}\left(\frac{\partial\tilde{\tilde{u}}_l^{(2)}}{\partial y_m}+\frac{\partial\tilde{\tilde{u}}_m^{(2)}}{\partial y_l}\right)\right] \right\rangle \\
& + \left\langle \frac{\partial\tilde{\tilde{p}}^{(1)}}{\partial\tau}, \frac{2\overline{\mu}}{3}\delta_{lm}\frac{\partial}{\partial y_m}\left[\tilde{\tilde{u}}_l^{(2)}\frac{\partial\tilde{\tilde{u}}_n^{(2)}}{\partial y_n}\right] \right\rangle + \left\langle \frac{\gamma-1}{2}\frac{\partial(\overline{p}^{(1)}+\tilde{\tilde{p}}^{(1)})\tilde{\tilde{u}}_k^{2,(1)}}{\partial\tau}, \frac{\partial\tilde{\tilde{p}}^{(2)}}{\partial\tau} \right\rangle + \left\langle \frac{\gamma-1}{2}\frac{\partial(\overline{p}^{(1)}+\tilde{\tilde{p}}^{(1)})\tilde{\tilde{u}}_k^{2,(1)}}{\partial\tau}, \frac{\gamma-1}{2}\frac{\partial(\overline{p}^{(2)}+\tilde{\tilde{p}}^{(2)})\tilde{\tilde{u}}_n^{2,(2)}}{\partial\tau} \right\rangle \\
& + \left\langle \frac{\gamma-1}{2}\frac{\partial(\overline{p}^{(1)}+\tilde{\tilde{p}}^{(1)})\tilde{\tilde{u}}_k^{2,(1)}}{\partial\tau}, \gamma\frac{\partial\tilde{\tilde{u}}_m^{(2)}(\overline{p}^{(2)}+\tilde{\tilde{p}}^{(2)})}{\partial y_m} \right\rangle + \left\langle \frac{\gamma-1}{2}\frac{\partial(\overline{p}^{(1)}+\tilde{\tilde{p}}^{(1)})\tilde{\tilde{u}}_k^{2,(1)}}{\partial\tau}, \frac{\gamma-1}{2}\frac{\partial(\overline{p}^{(2)}+\tilde{\tilde{p}}^{(2)})\tilde{\tilde{u}}_m^{(2)}\tilde{\tilde{u}}_n^{(2)}\tilde{\tilde{u}}_n^{(2)}}{\partial y_m} \right\rangle \\
& + \left\langle \frac{\gamma-1}{2}\frac{\partial(\overline{p}^{(1)}+\tilde{\tilde{p}}^{(1)})\tilde{\tilde{u}}_k^{2,(1)}}{\partial\tau}, -(\gamma-1)\frac{\overline{c}_p\overline{\mu}}{\overline{\mathcal{P}r}}\frac{\partial}{\partial y_m}\left(\frac{\partial\tilde{\tilde{T}}^{(2)}}{\partial y_m}\right) \right\rangle + \left\langle \frac{\gamma-1}{2}\frac{\partial(\overline{p}^{(1)}+\tilde{\tilde{p}}^{(1)})\tilde{\tilde{u}}_k^{2,(1)}}{\partial\tau}, -(\gamma-1)\overline{\mu}\frac{\partial}{\partial y_m}\left[\tilde{\tilde{u}}_l^{(2)}\left(\frac{\partial\tilde{\tilde{u}}_l^{(2)}}{\partial y_m}+\frac{\partial\tilde{\tilde{u}}_m^{(2)}}{\partial y_l}\right)\right] \right\rangle \\
& + \left\langle \frac{\gamma-1}{2}\frac{\partial(\overline{p}^{(1)}+\tilde{\tilde{p}}^{(1)})\tilde{\tilde{u}}_k^{2,(1)}}{\partial\tau}, \frac{2\overline{\mu}}{3}\delta_{lm}\frac{\partial}{\partial y_m}\left[\tilde{\tilde{u}}_l^{(2)}\frac{\partial\tilde{\tilde{u}}_n^{(2)}}{\partial y_n}\right] \right\rangle + \left\langle \gamma\frac{\partial\tilde{\tilde{u}}_j^{(1)}(\overline{p}^{(1)}+\tilde{\tilde{p}}^{(1)})}{\partial y_j}, \frac{\partial\tilde{\tilde{p}}^{(2)}}{\partial\tau} \right\rangle + \left\langle \gamma\frac{\partial\tilde{\tilde{u}}_j^{(1)}(\overline{p}^{(1)}+\tilde{\tilde{p}}^{(1)})}{\partial y_j}, \frac{\gamma-1}{2}\frac{\partial(\overline{p}^{(2)}+\tilde{\tilde{p}}^{(2)})\tilde{\tilde{u}}_n^{2,(2)}}{\partial\tau} \right\rangle \\
& + \left\langle \gamma\frac{\partial\tilde{\tilde{u}}_j^{(1)}(\overline{p}^{(1)}+\tilde{\tilde{p}}^{(1)})}{\partial y_j}, \gamma\frac{\partial\tilde{\tilde{u}}_m^{(2)}(\overline{p}^{(2)}+\tilde{\tilde{p}}^{(2)})}{\partial y_m} \right\rangle + \left\langle \gamma\frac{\partial\tilde{\tilde{u}}_j^{(1)}(\overline{p}^{(1)}+\tilde{\tilde{p}}^{(1)})}{\partial y_j}, \frac{\gamma-1}{2}\frac{\partial(\overline{p}^{(2)}+\tilde{\tilde{p}}^{(2)})\tilde{\tilde{u}}_m^{(2)}\tilde{\tilde{u}}_n^{(2)}\tilde{\tilde{u}}_n^{(2)}}{\partial y_m} \right\rangle \\
& + \left\langle \gamma\frac{\partial\tilde{\tilde{u}}_j^{(1)}(\overline{p}^{(1)}+\tilde{\tilde{p}}^{(1)})}{\partial y_j}, -(\gamma-1)\frac{\overline{c}_p\overline{\mu}}{\overline{\mathcal{P}r}}\frac{\partial}{\partial y_m}\left(\frac{\partial\tilde{\tilde{T}}^{(2)}}{\partial y_m}\right) \right\rangle + \left\langle \gamma\frac{\partial\tilde{\tilde{u}}_j^{(1)}(\overline{p}^{(1)}+\tilde{\tilde{p}}^{(1)})}{\partial y_j}, -(\gamma-1)\overline{\mu}\frac{\partial}{\partial y_m}\left[\tilde{\tilde{u}}_l^{(2)}\left(\frac{\partial\tilde{\tilde{u}}_l^{(2)}}{\partial y_m}+\frac{\partial\tilde{\tilde{u}}_m^{(2)}}{\partial y_l}\right)\right] \right\rangle \\
& + \left\langle \gamma\frac{\partial\tilde{\tilde{u}}_j^{(1)}(\overline{p}^{(1)}+\tilde{\tilde{p}}^{(1)})}{\partial y_j}, \frac{2\overline{\mu}}{3}\delta_{lm}\frac{\partial}{\partial y_m}\left[\tilde{\tilde{u}}_l^{(2)}\frac{\partial\tilde{\tilde{u}}_n^{(2)}}{\partial y_n}\right] \right\rangle + \left\langle \frac{\gamma-1}{2}\frac{\partial(\overline{p}^{(1)}+\tilde{\tilde{p}}^{(1)})\tilde{\tilde{u}}_j^{(1)}\tilde{\tilde{u}}_k^{(1)}\tilde{\tilde{u}}_k^{(1)}}{\partial y_j}, \frac{\partial\tilde{\tilde{p}}^{(2)}}{\partial\tau} \right\rangle \\
& + \left\langle \frac{\gamma-1}{2}\frac{\partial(\overline{p}^{(1)}+\tilde{\tilde{p}}^{(1)})\tilde{\tilde{u}}_j^{(1)}\tilde{\tilde{u}}_k^{(1)}\tilde{\tilde{u}}_k^{(1)}}{\partial y_j}, \frac{\gamma-1}{2}\frac{\partial(\overline{p}^{(2)}+\tilde{\tilde{p}}^{(2)})\tilde{\tilde{u}}_n^{2,(2)}}{\partial\tau} \right\rangle + \left\langle \frac{\gamma-1}{2}\frac{\partial(\overline{p}^{(1)}+\tilde{\tilde{p}}^{(1)})\tilde{\tilde{u}}_j^{(1)}\tilde{\tilde{u}}_k^{(1)}\tilde{\tilde{u}}_k^{(1)}}{\partial y_j}, \gamma\frac{\partial\tilde{\tilde{u}}_m^{(2)}(\overline{p}^{(2)}+\tilde{\tilde{p}}^{(2)})}{\partial y_m} \right\rangle \qquad (73) \\
& + \left\langle \frac{\gamma-1}{2}\frac{\partial(\overline{p}^{(1)}+\tilde{\tilde{p}}^{(1)})\tilde{\tilde{u}}_j^{(1)}\tilde{\tilde{u}}_k^{(1)}\tilde{\tilde{u}}_k^{(1)}}{\partial y_j}, \frac{\gamma-1}{2}\frac{\partial(\overline{p}^{(2)}+\tilde{\tilde{p}}^{(2)})\tilde{\tilde{u}}_m^{(2)}\tilde{\tilde{u}}_n^{(2)}\tilde{\tilde{u}}_n^{(2)}}{\partial y_m} \right\rangle + \left\langle \frac{\gamma-1}{2}\frac{\partial(\overline{p}^{(1)}+\tilde{\tilde{p}}^{(1)})\tilde{\tilde{u}}_j^{(1)}\tilde{\tilde{u}}_k^{(1)}\tilde{\tilde{u}}_k^{(1)}}{\partial y_j}, -(\gamma-1)\frac{\overline{c}_p\overline{\mu}}{\overline{\mathcal{P}r}}\frac{\partial}{\partial y_m}\left(\frac{\partial\tilde{\tilde{T}}^{(2)}}{\partial y_m}\right) \right\rangle \\
& + \left\langle \frac{\gamma-1}{2}\frac{\partial(\overline{p}^{(1)}+\tilde{\tilde{p}}^{(1)})\tilde{\tilde{u}}_j^{(1)}\tilde{\tilde{u}}_k^{(1)}\tilde{\tilde{u}}_k^{(1)}}{\partial y_j}, -(\gamma-1)\overline{\mu}\frac{\partial}{\partial y_m}\left[\tilde{\tilde{u}}_l^{(2)}\left(\frac{\partial\tilde{\tilde{u}}_l^{(2)}}{\partial y_m}+\frac{\partial\tilde{\tilde{u}}_m^{(2)}}{\partial y_l}\right)\right] \right\rangle + \left\langle \frac{\gamma-1}{2}\frac{\partial(\overline{p}^{(1)}+\tilde{\tilde{p}}^{(1)})\tilde{\tilde{u}}_j^{(1)}\tilde{\tilde{u}}_k^{(1)}\tilde{\tilde{u}}_k^{(1)}}{\partial y_j}, \frac{2\overline{\mu}}{3}\delta_{lm}\frac{\partial}{\partial y_m}\left[\tilde{\tilde{u}}_l^{(2)}\frac{\partial\tilde{\tilde{u}}_n^{(2)}}{\partial y_n}\right] \right\rangle \\
& + \left\langle -(\gamma-1)\overline{\mu}\frac{\partial}{\partial y_j}\left[\tilde{\tilde{u}}_i^{(1)}\left(\frac{\partial\tilde{\tilde{u}}_i^{(1)}}{\partial y_j}+\frac{\partial\tilde{\tilde{u}}_j^{(1)}}{\partial y_i}\right)\right], \frac{\partial\tilde{\tilde{p}}^{(2)}}{\partial\tau} \right\rangle + \left\langle -(\gamma-1)\overline{\mu}\frac{\partial}{\partial y_j}\left[\tilde{\tilde{u}}_i^{(1)}\left(\frac{\partial\tilde{\tilde{u}}_i^{(1)}}{\partial y_j}+\frac{\partial\tilde{\tilde{u}}_j^{(1)}}{\partial y_i}\right)\right], \frac{\gamma-1}{2}\frac{\partial(\overline{p}^{(2)}+\tilde{\tilde{p}}^{(2)})\tilde{\tilde{u}}_n^{2,(2)}}{\partial\tau} \right\rangle \\
& + \left\langle -(\gamma-1)\overline{\mu}\frac{\partial}{\partial y_j}\left[\tilde{\tilde{u}}_i^{(1)}\left(\frac{\partial\tilde{\tilde{u}}_i^{(1)}}{\partial y_j}+\frac{\partial\tilde{\tilde{u}}_j^{(1)}}{\partial y_i}\right)\right], \gamma\frac{\partial\tilde{\tilde{u}}_m^{(2)}(\overline{p}^{(2)}+\tilde{\tilde{p}}^{(2)})}{\partial y_m} \right\rangle + \left\langle -(\gamma-1)\overline{\mu}\frac{\partial}{\partial y_j}\left[\tilde{\tilde{u}}_i^{(1)}\left(\frac{\partial\tilde{\tilde{u}}_i^{(1)}}{\partial y_j}+\frac{\partial\tilde{\tilde{u}}_j^{(1)}}{\partial y_i}\right)\right], \frac{\gamma-1}{2}\frac{\partial(\overline{p}^{(2)}+\tilde{\tilde{p}}^{(2)})\tilde{\tilde{u}}_m^{(2)}\tilde{\tilde{u}}_n^{(2)}\tilde{\tilde{u}}_n^{(2)}}{\partial y_m} \right\rangle \\
& + \left\langle -(\gamma-1)^2\overline{\mu}\frac{\partial}{\partial y_j}\left[\tilde{\tilde{u}}_i^{(1)}\left(\frac{\partial\tilde{\tilde{u}}_i^{(1)}}{\partial y_j}+\frac{\partial\tilde{\tilde{u}}_j^{(1)}}{\partial y_i}\right)\right], -\frac{\overline{c}_p\overline{\mu}}{\overline{\mathcal{P}r}}\frac{\partial}{\partial y_m}\left(\frac{\partial\tilde{\tilde{T}}^{(2)}}{\partial y_m}\right) \right\rangle + \left\langle -(\gamma-1)^2\overline{\mu}\frac{\partial}{\partial y_j}\left[\tilde{\tilde{u}}_i^{(1)}\left(\frac{\partial\tilde{\tilde{u}}_i^{(1)}}{\partial y_j}+\frac{\partial\tilde{\tilde{u}}_j^{(1)}}{\partial y_i}\right)\right], -\overline{\mu}\frac{\partial}{\partial y_m}\left[\tilde{\tilde{u}}_l^{(2)}\left(\frac{\partial\tilde{\tilde{u}}_l^{(2)}}{\partial y_m}+\frac{\partial\tilde{\tilde{u}}_m^{(2)}}{\partial y_l}\right)\right] \right\rangle \\
& + \left\langle -(\gamma-1)\overline{\mu}\frac{\partial}{\partial y_j}\left[\tilde{\tilde{u}}_i^{(1)}\left(\frac{\partial\tilde{\tilde{u}}_i^{(1)}}{\partial y_j}+\frac{\partial\tilde{\tilde{u}}_j^{(1)}}{\partial y_i}\right)\right], \frac{2\overline{\mu}}{3}\delta_{lm}\frac{\partial}{\partial y_m}\left[\tilde{\tilde{u}}_l^{(2)}\frac{\partial\tilde{\tilde{u}}_n^{(2)}}{\partial y_n}\right] \right\rangle + \left\langle \frac{2\overline{\mu}}{3}\delta_{ij}\frac{\partial}{\partial y_j}\left[\tilde{\tilde{u}}_i^{(1)}\frac{\partial\tilde{\tilde{u}}_k^{(1)}}{\partial y_k}\right], \frac{\partial\tilde{\tilde{p}}^{(2)}}{\partial\tau} \right\rangle \\
& + \left\langle \frac{2\overline{\mu}}{3}\delta_{ij}\frac{\partial}{\partial y_j}\left[\tilde{\tilde{u}}_i^{(1)}\frac{\partial\tilde{\tilde{u}}_k^{(1)}}{\partial y_k}\right], \frac{\gamma-1}{2}\frac{\partial(\overline{p}^{(2)}+\tilde{\tilde{p}}^{(2)})\tilde{\tilde{u}}_n^{2,(2)}}{\partial\tau} \right\rangle + \left\langle \frac{2\overline{\mu}}{3}\delta_{ij}\frac{\partial}{\partial y_j}\left[\tilde{\tilde{u}}_i^{(1)}\frac{\partial\tilde{\tilde{u}}_k^{(1)}}{\partial y_k}\right], \gamma\frac{\partial\tilde{\tilde{u}}_m^{(2)}(\overline{p}^{(2)}+\tilde{\tilde{p}}^{(2)})}{\partial y_m} \right\rangle \\
& + \left\langle \frac{2\overline{\mu}}{3}\delta_{ij}\frac{\partial}{\partial y_j}\left[\tilde{\tilde{u}}_i^{(1)}\frac{\partial\tilde{\tilde{u}}_k^{(1)}}{\partial y_k}\right], \frac{\gamma-1}{2}\frac{\partial(\overline{p}^{(2)}+\tilde{\tilde{p}}^{(2)})\tilde{\tilde{u}}_m^{(2)}\tilde{\tilde{u}}_n^{(2)}\tilde{\tilde{u}}_n^{(2)}}{\partial y_m} \right\rangle + \left\langle \frac{2\overline{\mu}}{3}\delta_{ij}\frac{\partial}{\partial y_j}\left[\tilde{\tilde{u}}_i^{(1)}\frac{\partial\tilde{\tilde{u}}_k^{(1)}}{\partial y_k}\right], -(\gamma-1)\frac{\overline{c}_p\overline{\mu}}{\overline{\mathcal{P}r}}\frac{\partial}{\partial y_m}\left(\frac{\partial\tilde{\tilde{T}}^{(2)}}{\partial y_m}\right) \right\rangle \\
& + \left\langle \frac{2\overline{\mu}}{3}\delta_{ij}\frac{\partial}{\partial y_j}\left[\tilde{\tilde{u}}_i^{(1)}\frac{\partial\tilde{\tilde{u}}_k^{(1)}}{\partial y_k}\right], -(\gamma-1)\overline{\mu}\frac{\partial}{\partial y_m}\left[\tilde{\tilde{u}}_l^{(2)}\left(\frac{\partial\tilde{\tilde{u}}_l^{(2)}}{\partial y_m}+\frac{\partial\tilde{\tilde{u}}_m^{(2)}}{\partial y_l}\right)\right] \right\rangle + \left\langle \frac{2\overline{\mu}}{3}\delta_{ij}\frac{\partial}{\partial y_j}\left[\tilde{\tilde{u}}_i^{(1)}\frac{\partial\tilde{\tilde{u}}_k^{(1)}}{\partial y_k}\right], \frac{2\overline{\mu}}{3}\delta_{lm}\frac{\partial}{\partial y_m}\left[\tilde{\tilde{u}}_l^{(2)}\frac{\partial\tilde{\tilde{u}}_n^{(2)}}{\partial y_n}\right] \right\rangle.
\end{aligned}
$$

References

[1]Taylor, G. I., "Statistical Theory of Turbulence," *Proc. R. Soc. Lond. A*, Vol. 151, No. 873, 1935, pp. 421–444. doi:10.1098/rspa.1935.0158.

[2]Kolmogorov, A. N., "The Local Structure of Turbulence in Incompressible Viscous Fluid for Very Large Reynolds Number," *Dokl. Akad. Nauk. SSSR*, Vol. 30, 1941, pp. 299–303.

[3]Kolmogorov, A. N., "On Degeneration of Isotropic Turbulence in an Incompressible Viscous Liquid," *Dokl. Akad. Nauk. SSSR*, Vol. 31, 1941, pp. 147.

[4]Kolmogorov, A. N., "Dissipation of Energy in Locally Isotropic Turbulence," *Dokl. Akad. Nauk. SSSR*, Vol. 32, 1941, pp. 19–21.

[5]Readhead, C. S. and Lawrence, C. R., "Observations of the Isotropy of the Cosmic Microwave Background Radiation," *Annual Review of Astronomy and Astrophysics*, Vol. 30, No. 1, 1992, pp. 653–703. doi:10.1146/annurev.aa.30.090192.003253.

[6]Hesselink, L. and Sturtevant, B., "Propagation of Weak Shocks Through a Random Medium," *Journal of Fluid Mechanics*, Vol. 196, 1988, pp. 513–553. doi:10.1017/s0022112088002800.

[7]Stewart, R. W. and Townsend, A. A., "Similarity and Self-Preservation in Isotropic Turbulence," *The Royal Society: Philosophical Transactions A*, Vol. 243, No. 867, 1951, pp. 359–385. doi:10.1098/rsta.1951.0007.

[8]Sreenivasan, K. R. and Antonia, R. A., "The Phenomenology of Small-Scale Turbulence," *Annual Review of Fluid Mechanics*, Vol. 29, 1997, pp. 435–472. doi:10.1146/annurev.fluid.29.1.435.

[9]Ishihara, T., Gotoh, T., and Kaneda, Y., "Study of High-Reynolds Number Isotropic Turbulence by Direct Numerical Simulation," *Annual Review of Fluid Mechanics*, Vol. 41, 2009, pp. 165–180. doi:10.1146/annurev.fluid.010908.165203.

[10]Pope, S. B., "Turbulent Flows," *Cambridge University Press*, 2000.

[11]Kolmogorov, A. N., "A Refinement of Previous Hypotheses Concerning the Local Structure of Turbulence in a Viscous Incompressible Fluid at High Reynolds Number," *Colloque International du C.N.R.S. de Mcanique de la Turbulence, Marseilles*, Aug/Sept 1961, pp. 453–458.

[12]Batchelor, G. K., "Pressure Fluctuations in Isotropic Turbulence," *Mathematical Proceedings of the Cambridge Philosophical Society*, Vol. 47, No. 2, 1951, pp. 359–374. doi:10.1017/S0305004100026712.

[13]Hill, R. J. and Wilczak, J. M., "Pressure Structure Functions and Spectra for Locally Isotropic Turbulence," *Journal of Fluid Mechanics*, Vol. 296, 1995, pp. 247–269. doi:10.1017/S0022112095002126.

[14]Gotoh, T. and Rogallo, R. S., "Statistics of Pressure and Pressure Gradient in Homogeneous Isotropic Turbulence," *Center for Turbulence Research, Proceedings of the Summer Program*, 1994, pp. 189–205.

[15]Albertson, J. D., Katul, G. G., Parlange, M. B., and Eichinger, W. E., "Spectral Scaling of Static Pressure Fluctuations in the Atmospheric Surface Layer: The Interaction Between Large and Small Scales," *Physics of Fluids*, Vol. 10, No. 7, 1998, pp. 1725–1932. doi:10.1063/1.869689.

[16]Patwardhan, S. S. and Ramesh, O. N., "Scaling of Pressure Spectrum in Turbulent Boundary Layers," *Journal of Physics: Conference Series*, Vol. 506, No. 012011, 2014, pp. 1–10. doi:10.1088/1742-6596/506/1/012011.

[17]Corrsin, S., "The Decay of Isotropic Temperature Fluctuations in an Isotropic Turbulence," *Journal of the Aeronautical Sciences*, Vol. 18, 1951, pp. 417–423. doi:10.2514/8.1982.

[18]Corrsin, S., "On the Spectrum of Isotropic Temperature Fluctuations in an Isotropic Turbulence," *Journal of Applied Physics*, Vol. 22, No. 4, 1951, pp. 469–473. doi:10.1063/1.1699986.

[19]Lesieur, M., Montmory, C., and Chollett, J. P., "The Decay of Kinetic Energy and Temperature Variance in Three-Dimensional Isotropic Turbulence," *Physics of Fluids*, Vol. 30, No. 5, 1987, pp. 1278–1286. doi:10.1063/1.866295.

[20]Lewalle, J., "Decay of Velocity and Temperature Fluctuations in Grid Turbulence," *AIAA Journal*, Vol. 28, No. 1, 1990, pp. 106–112. doi:10.2514/3.10359.

[21]Sreenivasan, K. R., Tavoularis, S., Henry, R., and Corrsin, S., "Temperature Fluctuations and Scales in Grid-Generated Turbulence," *Journal of Fluid Mechanics*, Vol. 100, No. 3, 1980, pp. 597–621. doi:10.1017/S0022112080001309.

[22]Chandrasekhar, S., "The Fluctuations of Density in Isotropic Turbulence," *Proceedings of the Royal Society of London. Series A, Mathematical and Physical Sciences*, Vol. 210, No. 1100, 1951, pp. 18–25. doi:10.1098/rspa.1951.0227.

[23]Montgomery, D., Brown, M. R., and Matthaeus, W. H., "Density Fluctuation Spectra in Magnetohydrodynamic Turbulence," *Journal of Geophysical Research*, Vol. 92, No. A1, 1987, pp. 282–284. doi:10.1029/JA092iA01p00282.

[24]Reid, W. H. and Harris, D. L., "Similarity Spectra in Isotropic Turbulence," *Physics of Fluids*, Vol. 2, No. 2, 1959, pp. 139–146. doi:10.1063/1.1705904.

[25]Proudman, I., "The Generation of Noise by Isotropic Turbulence," *The Royal Society: Proceedings A*, Vol. 214, No. 1116, 1952, pp. 119–132. doi:10.1098/rspa.1952.0154.

[26]Lighthill, M. J., "Aerodynamic Noise, or, Turbulence as a Source of Sound," *Fluid Motion Sub-Committee Aeronautical Research Council*, 1950, pp. 1–26.

[27]Lighthill, M. J., "On Sound Generated Aerodynamically. I. General Theory," *Proc. R. Soc. Lond. A.*, Vol. 211, No. 1107, 1952, pp. 564–587. doi:10.1098/rspa.1952.0060.

[28]Lighthill, M. J., "On Sound Generated Aerodynamically. II. Turbulence as a Source of Sound," *Proc. R. Soc. Lond. A.*, Vol. 222, No. 1148, 1954, pp. 1–32. doi:10.1098/rspa.1954.0049.

[29]Lilley, G. M., "The Radiated Noise from Isotropic Turbulence Revisited," *NASA CR-191547*, 1993.

[30]Lilley, G. M., "The Acoustic Spectrum in the Sound Field of Isotropic Turbulence," *International Journal of Aeroacoustics*, Vol. 4, No. 1, 2005, pp. 11–20. doi:10.1260/1475472053730011.

[31]Lilley, G. M., "The Radiated Noise from Isotropic Turbulence with Applications to the Theory of Jet Noise," *Journal of Sound and Vibration*, Vol. 190, No. 3, 1996, pp. 463–476. doi:10.1006/jsvi.1996.0074.

[32]Passot, T. and Pouquet, A., "Numerical Simulation of Compressible Homogeneous Flows in the Turbulent Regime," *Journal of Fluid Mechanics*, Vol. 181, 1987, pp. 441–166. doi:10.1017/s0022112087002167.

[33]Mansour, N. N. and Wray, A. A., "Decay of Isotropic Turbulence at Low Reynolds Number," *Physics of Fluids. Fluids*, Vol. 6, No. 808, 1994, pp. 808–814. doi:10.1063/1.868319.

[34]Yao, H., He, G., Wang, M., and Zhang, X., "Time Correlations of Pressure in Isotropic Turbulence," *Physics of Fluids*, Vol. 20, No. 2, 2008, pp. 1–4. doi:10.1063/1.2870111.

[35]Langford, J. A. and Moser, R. D., "Optimal LES Formulations for Isotropic Turbulence," *Journal of Fluid Mechanics*, Vol. 398, 1999, pp. 321–346. doi:10.1017/s0022112099006369.

[36]Thornber, B., Mosedale, A., and Drikakis, D., "On the Implicit Large Eddy Simulations of Homogeneous Decaying Turbulence," *Journal of Computational Physics*, Vol. 226, No. 2, 2007, pp. 1902–1929. doi:10.1016/j.jcp.2007.06.030.

[37]Vreman, A. W., Geurts, B. J., Kuerten, J. G. M., and Zandbergen, P. J., "A Finite Volume Approach to Large Eddy Simulation of Compressible, Homogeneous, Isotropic, Decaying Turbulence," *International Journal for Numerical Methods in Fluids*, Vol. 15, No. 7, 1992, pp. 799–816. doi:10.1002/fld.1650150705.

[38]Abdibekov, U. S. and Zhakebaev, D. B., "Modelling of the Decay of Isotropic Turbulence by the LES," *Journal of Physics Conference Series*, Vol. 318, No. 4, 2011. doi:10.1088/1742-6596/318/4/042042.

[39]Hughes, T. J. R., Mazzei, L., Oberai, A. A., and Wray, A., "The Multiscale Formulation of Large Eddy Simulation: Decay of Homogeneous Isotropic Turbulence," *Physics of Fluids*, Vol. 13, No. 2, 2001, pp. 505–512. doi:10.1063/1.1332391.

[40]Zang, T. A., Dahlburg, R. B., and Dahlburg, J. P., "Direct and Large-Eddy Simulations of Three-Dimensional Compressible Navier-Stokes Turbulence," *Physics of Fluids A: Fluid Dynamics*, Vol. 4, No. 1, 1992, pp. 127–140. doi:10.1063/1.858491.

[41]Swanson, R. C., Rumsey, C. L., Rubinstein, R., Balakumar, P., and Zang, T. A., "Parametric Study of Decay of Homogeneous Isotropic Turbulence using Large Eddy Simulation," *NASA TM-2012-217593*, 2012.

[42]Sarkar, S. and Hussaini, M. Y., "Computation of the Sound Generated by Isotropic Turbulence," *NASA-CR-191543*, 1993, pp. 1–30.

[43]Witkowska, A., Juve, D., and Brasseur, J. G., "Numerical Study of Noise from Isotropic Turbulence," *Journal of Computational Acoustics*, Vol. 5, No. 3, 1997, pp. 317–336. doi:10.1142/S0218396X97000186.

[44]Seror, C., Sagaut, P., Bailly, C., and Juve, D., "On the Radiated Noise Computed by Large-Eddy Simulation," *Physics of Fluids*, Vol. 13, No. 476, 2001, pp. 476–487. doi:10.1063/1.1336150.

[45]Zhou, Y. and Dong, Y., "An Investigation of the Lattice Boltzmann Equation-Based Hybrid Approach for Simulation of Sound Generated by Isotropic Turbulence," *Computers and Fluids*, Vol. 100, 2014, pp. 267–277. doi:10.1016/j.compfluid.2014.05.015.

[46]Wiener, N., "Time Series," *MIT Press*, 1964.

[47]Lighthill, M. J., "Viscosity Effects in Sound Waves of Finite Amplitude," *Survey of Mechanics, ed. by Batchelor, G. K. and Davies, R. M.*, 1956, pp. 249–350.

[48]Debussche, A., Dubois, T., and Temam, R., "The Nonlinear Galerkin Method: A Multi-Scale Method Applied to the Simulation of Homogeneous Turbulent Flows," *ICASE Report 93/93*, 1993.

Figures

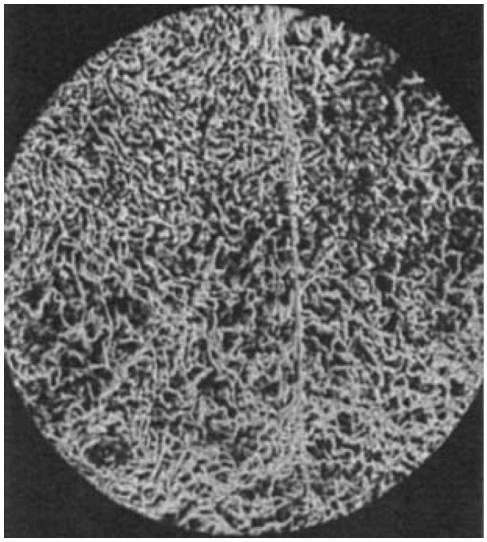

(a) Schlieren

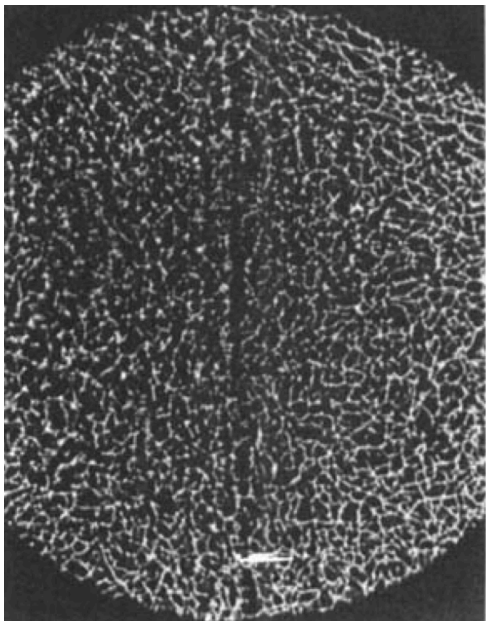

(b) Shadow graph

Figure 1. Photographs of a Mach 1.03 shock moving through isotropic turbulence. Courtesy of Hesselink and Sturtevant.[6]

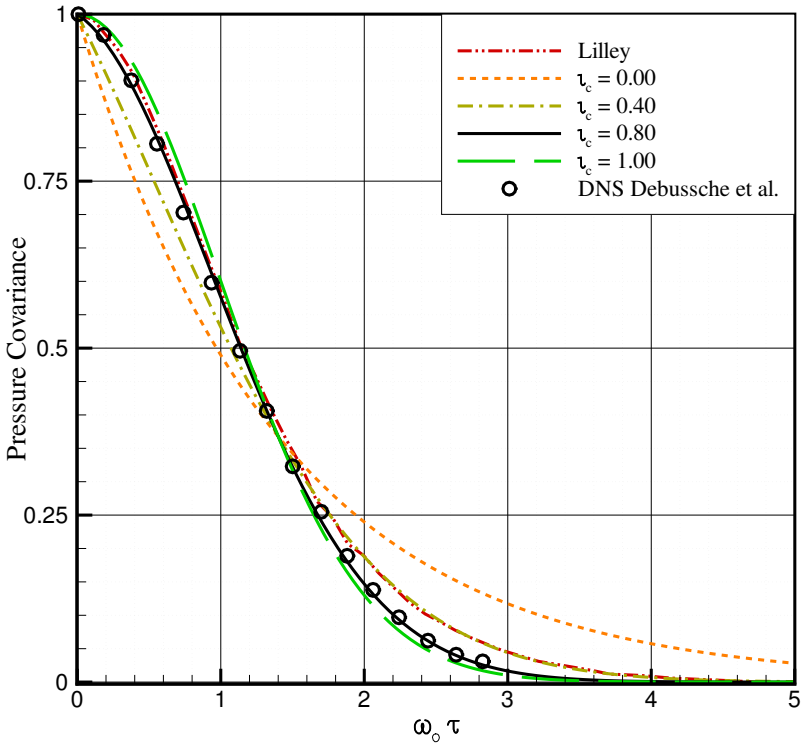

Figure 2. The decay of pressure covariance.

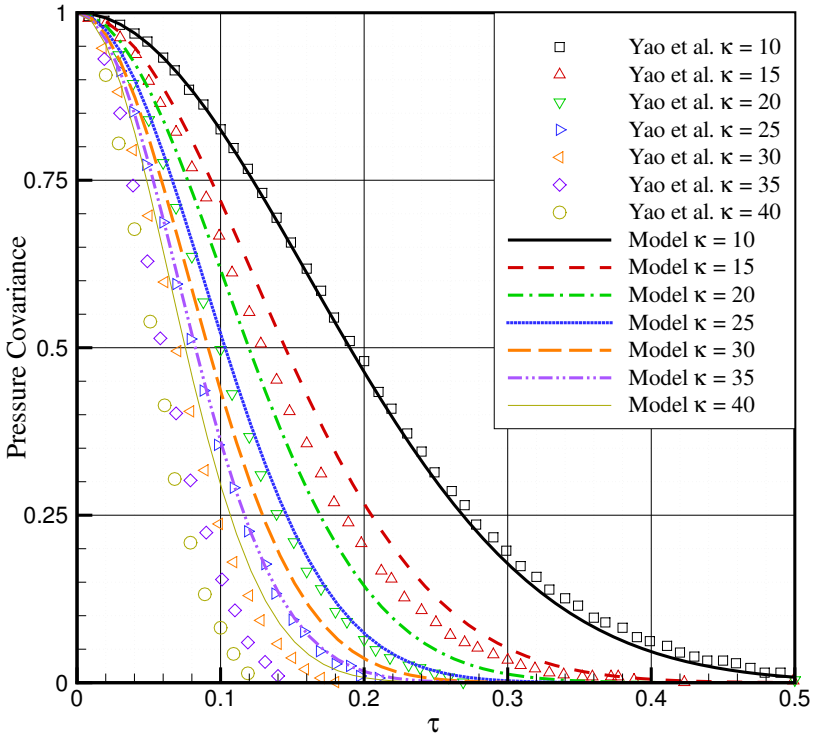

Figure 3. Decay of auto-correlation of pressure on a wavenumber basis for stationary turbulence at $\mathcal{R}e_\lambda = 78.75$.

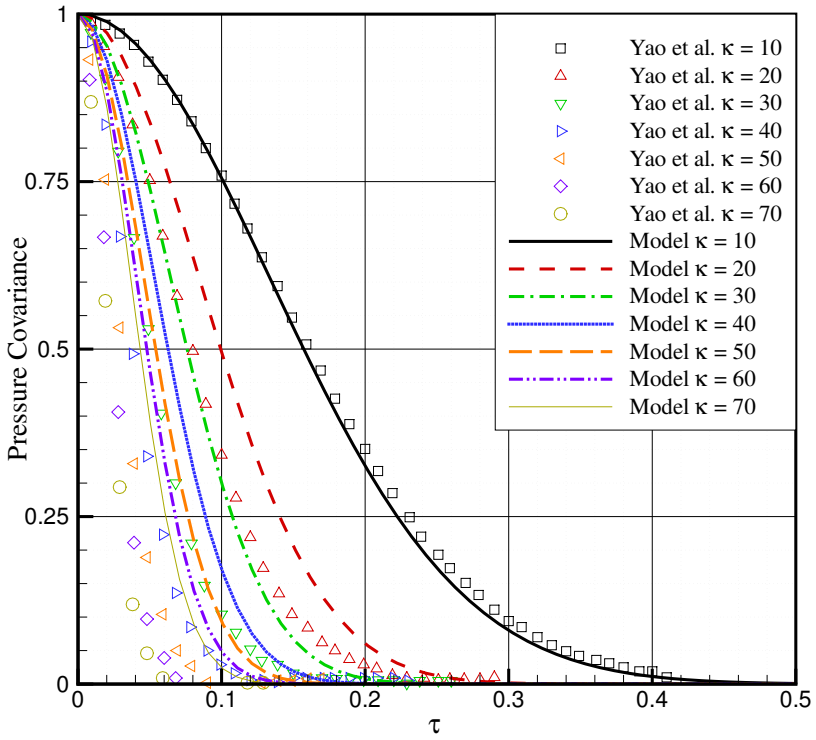

Figure 4. Decay of auto-correlation of pressure on a wavenumber basis for stationary turbulence at $\mathcal{R}e_\lambda = 148.92$.

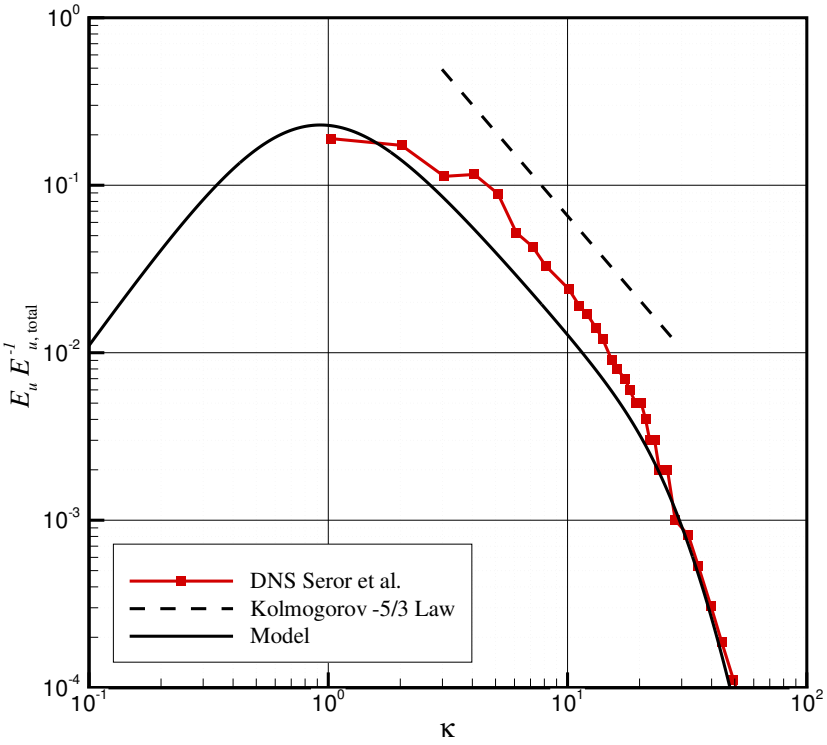

Figure 5. The spectrum of E_u normalized by the total energy of E_u in the wavenumber domain.

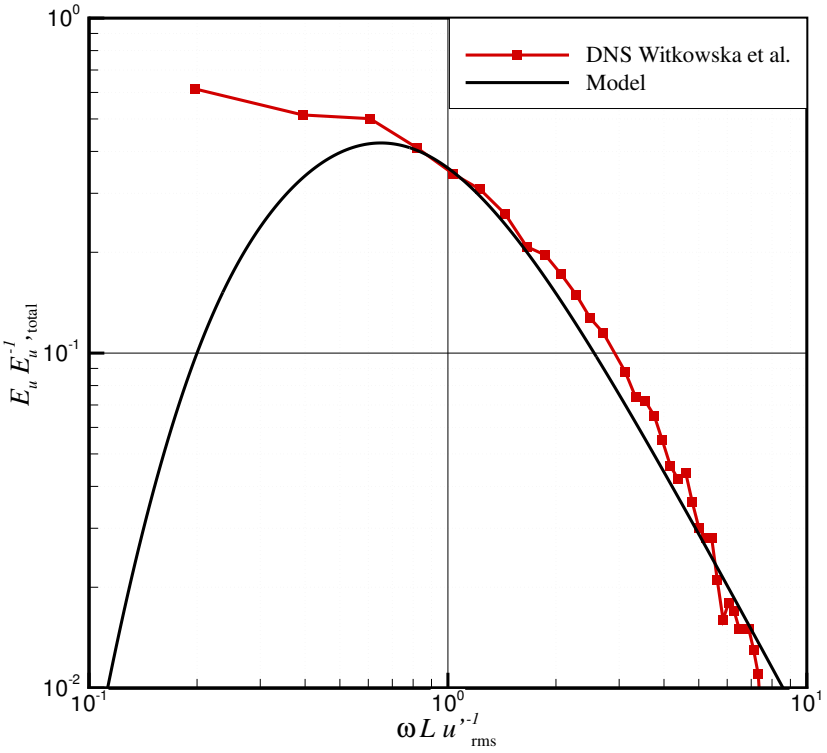

Figure 6. The spectrum of E_u normalized by the total energy of E_u in the frequency domain.

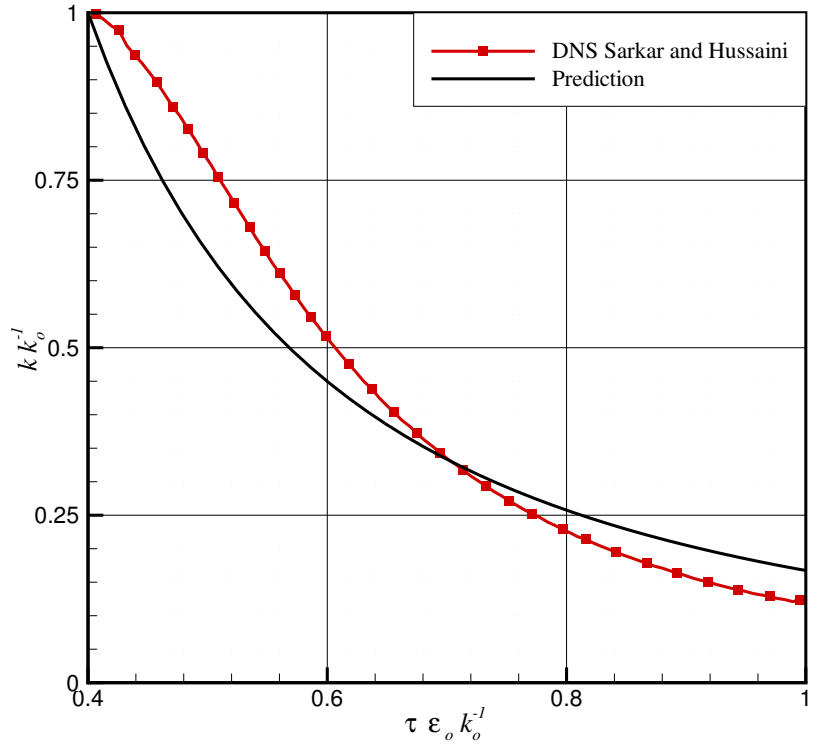

Figure 7. Normalized k within decaying isotropic turbulence.

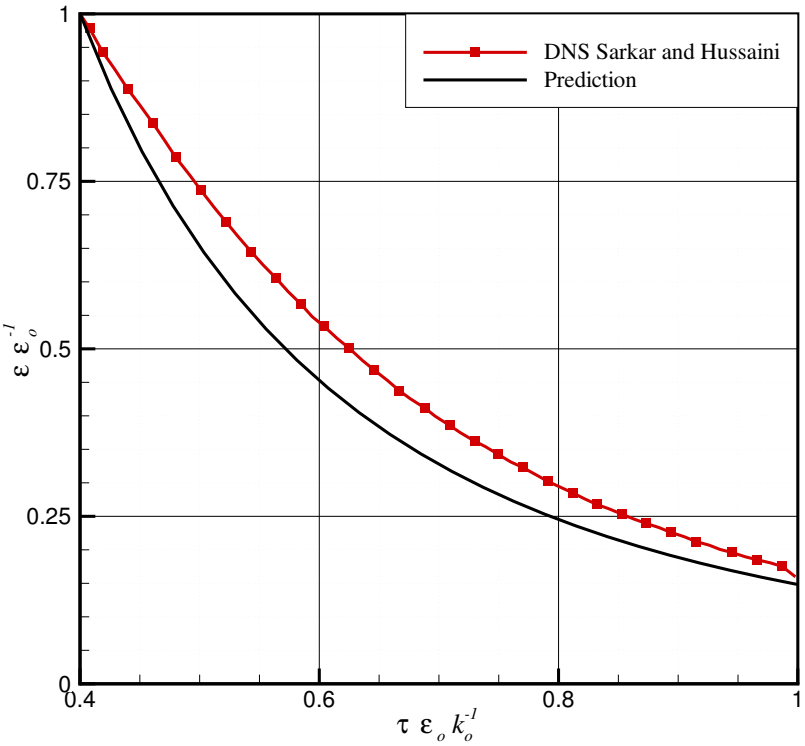

Figure 8. Normalized ϵ within decaying isotropic turbulence.

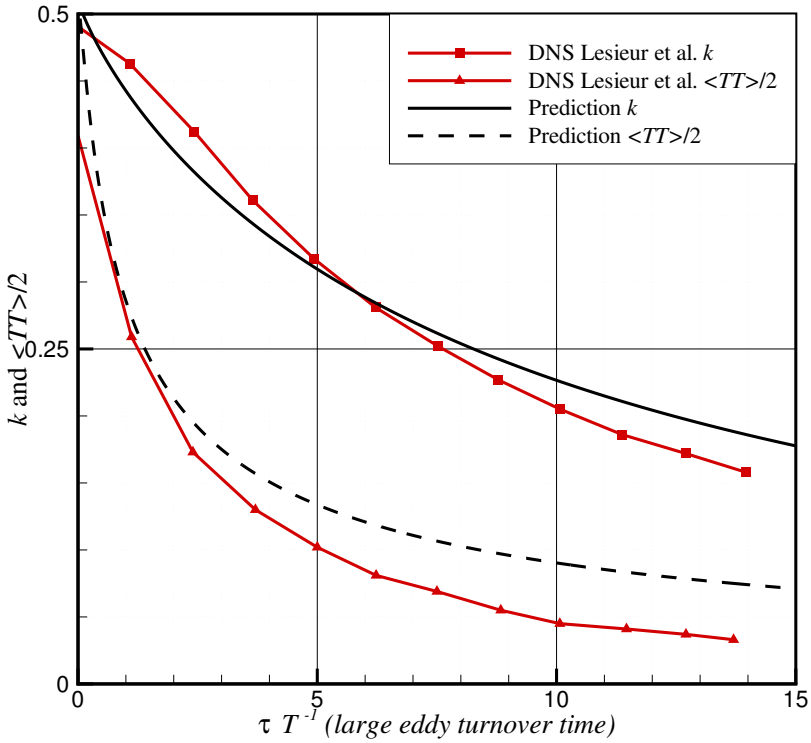

Figure 9. Decay of k and $< TT > /2$ with increasing time τ.

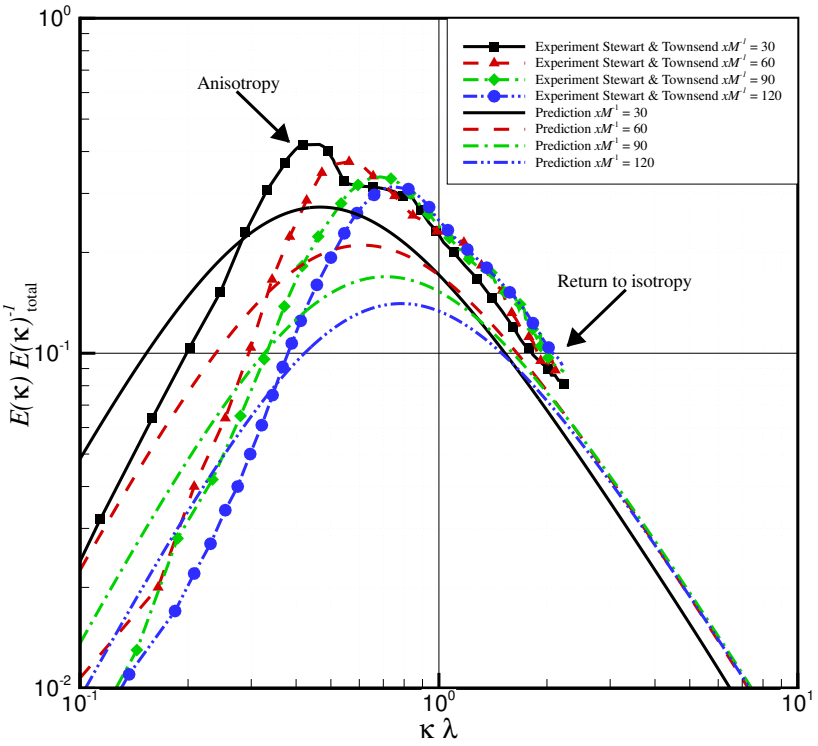

Figure 10. Wavenumber energy spectrum, $E_u(\kappa)$, at various axial distances within grid turbulence.

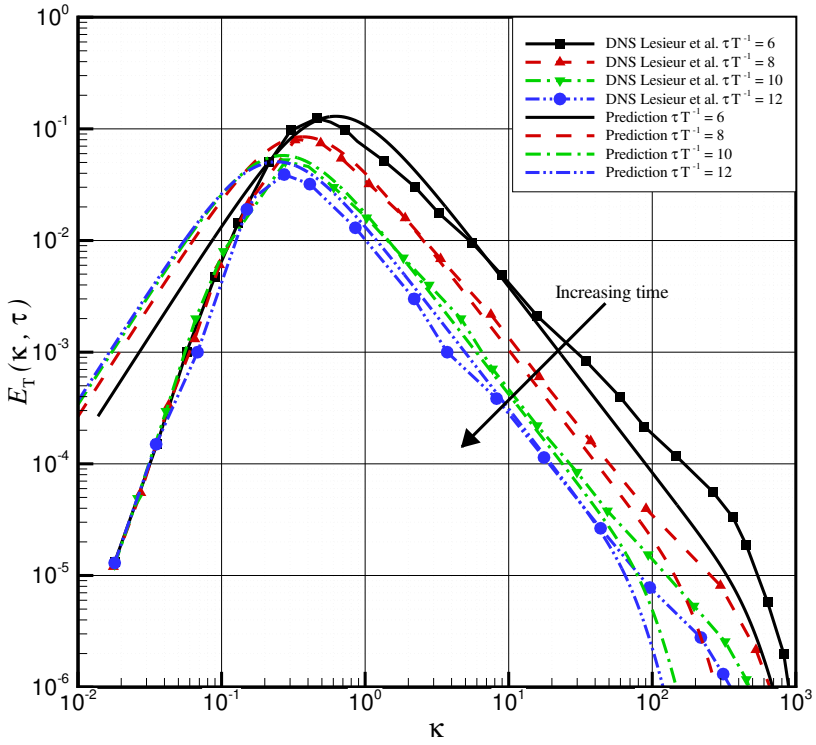

Figure 11. Wavenumber spectrum, $E_T(\kappa)$, within decaying isotropic turbulence at various large-eddy turn-over times.

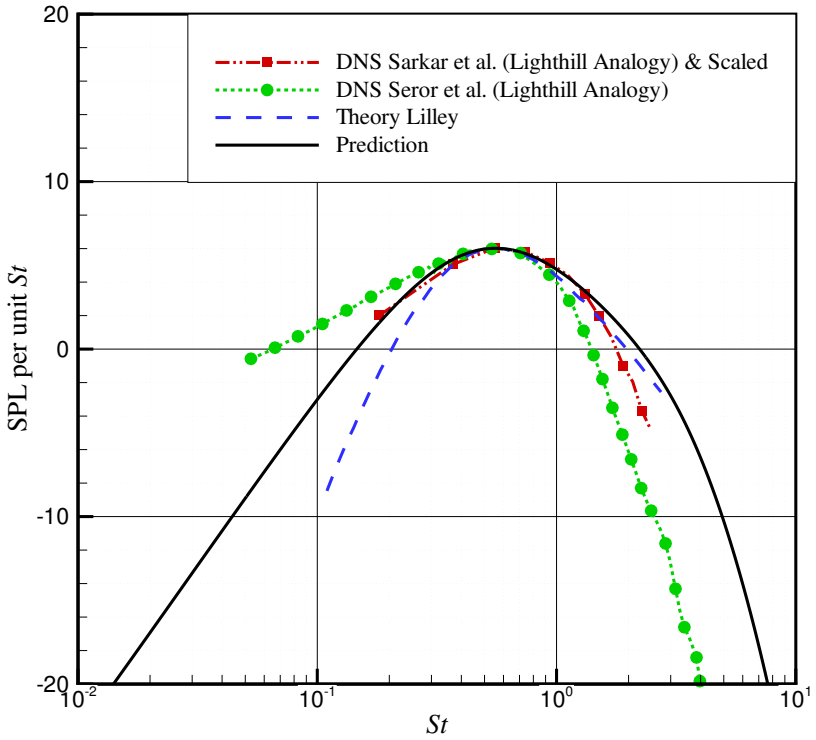

Figure 12. The power spectrum of acoustic pressure.

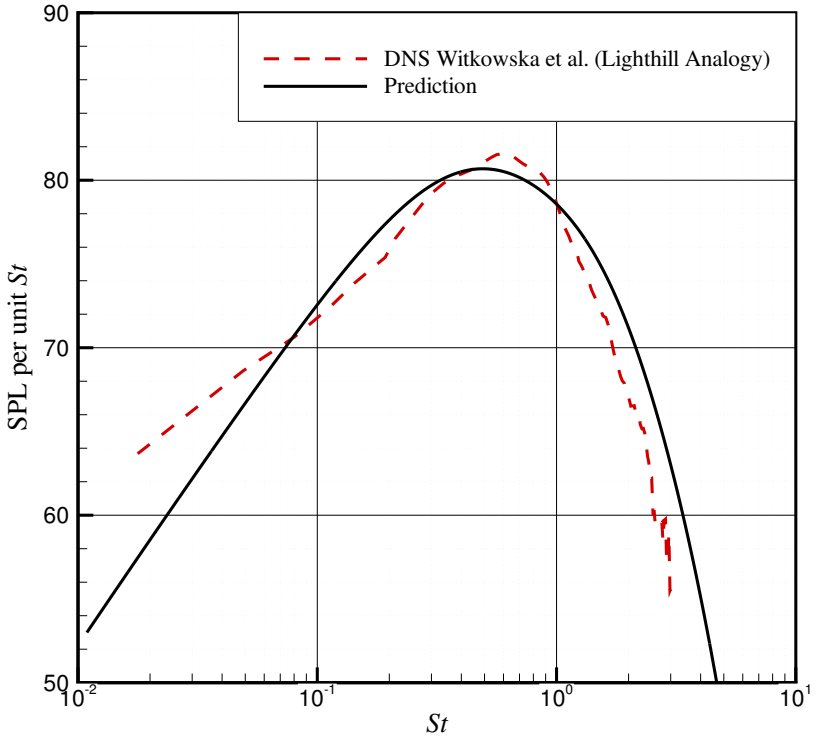

Figure 13. The power spectrum of acoustic pressure.

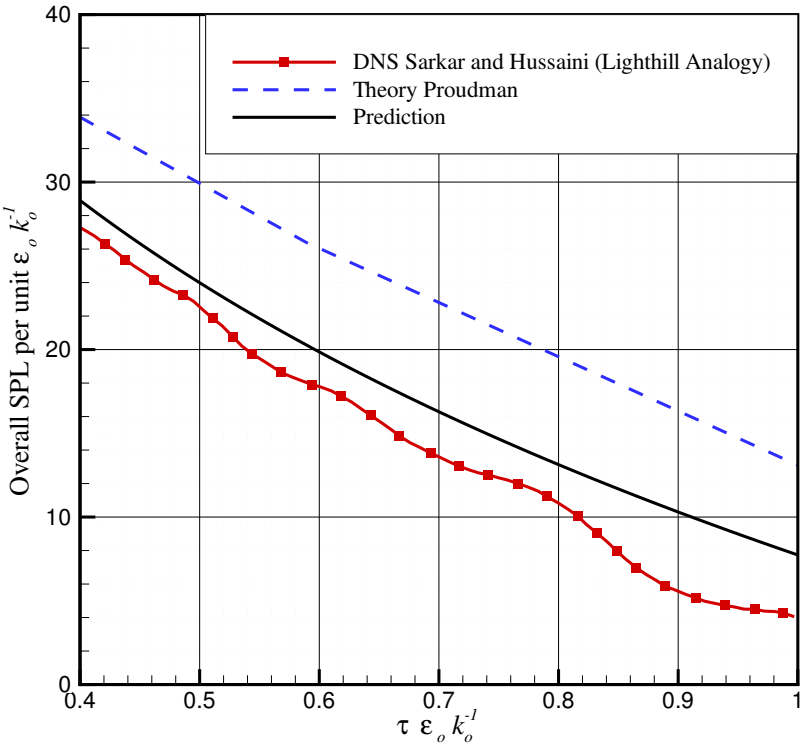

Figure 14. Acoustic OASPL per unit $\epsilon_o k_o^{-1}$ from decaying isotropic turbulence.